

N69-24893

(ACCESSION NUMBER)

78

(THRU)

1

(PAGES)

Oct 10 1982

(CODE)

30

(CATEGORY)

JET PROPULSION LABORATORY
CALIFORNIA INSTITUTE OF TECHNOLOGY
PASADENA, CALIFORNIA

RE-ORDER NO. 68-593

09349-6001-R000

TECHNICAL REPORT

MARS SURFACE SOIL
EROSION STUDY

CONTRACT NO. AX 422060

FEBRUARY 28, 1968

Prepared By
Robert E. Hutton

for

JET PROPULSION LABORATORY
CALIFORNIA INSTITUTE OF TECHNOLOGY
Pasadena, California

This work was performed for the Jet Propulsion Laboratory,
California Institute of Technology, sponsored by the
National Aeronautics and Space Administration under
Contract NAS7-100.

ACKNOWLEDGMENTS

The author wishes to express his appreciation to F. C. Vote and J. R. Wrobel of Jet Propulsion Laboratories for the helpful technical discussions during the performance of this study.

CONTENTS

	Page
1. SUMMARY	1
2. INTRODUCTION.....	3
3. RESULTS	5
3.1 Surface Loadings	6
3.2 Soil Erosion	16
3.3 Soil Particle Displacements	22
4. REFERENCES	R-1

APPENDICES

A ROBERTS' THEORY.....	A-1
1. Definition of Symbols	A-3
2. Governing Equations	A-5
3. Modifications of Roberts' Theory	A-7
4. FORTRAN IV Soil Erosion Program	A-8
5. Example FORTRAN IV Soil Erosion Calculations .	A-28
B JET TURNING ANGLE	B-1
C PARTICLE TRAJECTORIES.....	C-1

ILLUSTRATIONS

	Page
1. Variations of Surface Pressure With Nozzle Height (vacuum expansion)	7
2. Variation of Gas Radial Velocity Along the Surface Height (vacuum expansion)	8
3. Variation of Retro-Rocket Exhaust Gas Density Along the Surface (vacuum expansion)	9
4. Variation of Dynamic Pressure With Nozzle Height (vacuum expansion)	10
5. Variation of Surface Pressure With Nozzle Height ($n = 2.15$)	12
6. Variation of Gas Radial Velocity Along the Surface With Nozzle Height ($n = 2.15$)	13
7. Variation of Retro-Rocket Exhaust Gas Density Along the Surface ($n = 2.15$)	14
8. Variation of Dynamic Pressure With Nozzle Height ($n = 2.15$)	15
9. Variation of Maximum Soil Erosion Rate With Soil Cohesion and Particle Size (nozzle height = 5 ft, vacuum expansion)	17
10. Erosion Profile in a Cohesionless Soil for Various Engine Thrust Cutoff Heights (300 micron diameter soil particles, vacuum expansion)	18
11. Erosion Profile for Various Engine Thrust Cutoff Heights (300 micron diameter particles, 0.072 psf cohesion, vacuum expansion)	19
12. Erosion Profile in a Cohesionless Soil for Various Engine Thrust Cutoff Heights (50 micron diameter soil particles, vacuum expansion)	20
13. Erosion Profile in a Cohesionless Soil for Various Engine Thrust Cutoff Heights (10 micron diameter soil particles, vacuum expansion)	21
14. Erosion Profile in a Cohesionless Soil for Various Engine Thrust Cutoff Heights (300 micron diameter soil particles) ($n = 2.15$)	23

ILLUSTRATIONS (continued)

	Page
15. Erosion Profile for Various Engine Thrust Cutoff Heights (300 micron diameter particles, 0.072 psf cohesion, n=2.15)	24
16. Variation of Debris Impact Point With Particle Diameter and Engine Thrust Cutoff Height (Cohesionless Soil)	27

1. SUMMARY

An analytical investigation was conducted to estimate the Martian surface loadings, soil erosion and the distances that soil debris is ejected as a result of the firing of the terminal descent rocket engine during a landing on the Martian surface. Theoretical surface loadings exhaust gas densities were computed for engine heights of 5, 10, 15, and 20 feet for the system parameters provided by Jet Propulsion Laboratories (JPL). Soil erosion rates and crater profiles were computed for Martian soils composed of 10, 50, and 300 micron diameter particles for cohesionless and cohesive soils. The erosion profile data are based on a 5 ft/sec vertical descent speed and engine thrust cutoff heights of 5, 10, 15, and 20 feet above the Martian surface. Data are also presented showing the distances along the surface that soil debris may be displaced because of soil erosion.

The computed data indicated the maximum surface excess pressure caused by gas impingement on the surface to be about 0.081 psi at the lowest nozzle height of 5 feet. This pressure is on the order of the estimated ambient pressure of 0.0726 psi provided by JPL at the Martian surface. The maximum jet gas density along the surface is about 10^{-6} slugs/ft³, which is smaller than the ambient density of about 7×10^{-5} slugs/ft³ estimated from the ambient pressure data provided by JPL.

The data further indicate soil erosion will be quite small and, in general, negligible. Maximum erosion depth occurs for a soil composed of 300 micron diameter particles for the lowest thrust cutoff height of 5 feet. In a cohesionless soil, the maximum erosion depth is about 0.02 inch. Jet focusing, because of the Martian ambient pressure, may cause deeper erosions. Erosion depth data obtained for an estimate of the focusing effect indicated the maximum erosion may be increased from 0.02 to 0.05 inch. For the 10 and 50 micron diameter particles and the soil cohesion values provided by JPL, the gas viscous shear stresses were less than the soil restraint capability and therefore, no erosion takes place. If the soil is considered completely cohesionless, some erosion does occur, but the depths are smaller than in the soil composed of 300 micron diameter particles.

The surface debris displaced in a cohesive soil extends out to about 24 feet (about the radius of the erosion profile). For the cohesionless soils, the small diameter particles are accelerated to a large fraction of the gas velocity and may be displaced to about 120 feet from the stagnation point. However, if the local variations of the surface are such that soil particles depart from the surface at angles much steeper than the slope of the erosion crater, they could be displaced to much larger distances. Theoretically, at the entrained velocities of the 300 micron diameter particles and a departure angle of 15 degrees, the ballistic trajectory in a perfect vacuum would displace them about 5000 feet. Nevertheless, the Martian atmosphere would significantly reduce this range. Based on the theory developed in Appendix C and the estimated value of the drag coefficient and Martian atmospheric density, atmosphere drag would reduce the range to about 1400 feet. Most likely, such ranges are extreme upper bounds, and a more reasonable range for debris displacement may be more nearly 100 feet from the stagnation point. It should be noted that debris ejected from the lunar surface, during the translational maneuver on Surveyor VI, did not indicate any large surface erosions nor ejection of debris to large distances. During that maneuver, the predicted surface loadings were at least an order of magnitude higher than those predicted here during the descent to the Martian surface, primarily because the Surveyor vernier engine was much closer to the surface.

2. INTRODUCTION

When retro-rocket engines are used to produce the braking force required to effect a soft landing on the Martian surface, the exhaust gases produce surface loadings which may cause surface erosion, the ejection of surface debris, and also the diffusion of exhaust gases into the porous surface. The amount of erosion depends on the magnitude of the erosive forces caused by the gas, and the resistance of the surface to such erosive forces. A theoretical formulation of this phenomena was considered in References 1 and 2 for a rocket engine thrusting in the near perfect vacuum found on the moon while the jet gases impinge perpendicularly onto a surface composed of soil particles. The gas flow field created by the interaction of the impinging gases and soil surface is axisymmetric about the stagnation point, and the corresponding radial flow of the gas along the soil surface produces shear stresses on the soil. If these shear stresses exceed the shear resistance of the soil, soil particles become entrained in the flowing gas and are transported in the direction of flow, thereby forming an erosion crater in the soil. Eventually the (entrained) soil particles fall back to the surface under the influence of gravity.

Since the gravitational acceleration field is higher on Mars than on the Moon, the resistance to erosion caused by friction between soil particles is larger on Mars. On the other hand, the finite, although small, atmosphere on Mars may cause a focusing of the jet exhaust gases and thereby produce larger erosive forces on the Martian surface than would be developed by the same engine in the lunar environment. The specific dependence of surface loadings on ambient pressure is not known and is being investigated experimentally at the present time by a joint effort of JPL and Langley Research Center (LRC).

The work presented in this investigation uses the theory in References 1 and 2 to make an engineering assessment of the soil erosion during touchdown on Mars. Since it is recognized the possibility exists that the finite atmosphere existing on Mars will cause a focusing of the jet gases and influence soil erosion, a modification was made to the theory by the introduction of an additional nondimensional parameter, n (Appendix A). The validity of this procedure and the value of the nondimensional parameter can be determined when data from the current test program become available.

The next section presents data showing the surface loadings caused by the retro-rocket gases at 5, 10, 15, and 20 foot nozzle heights above the Martian surface for vacuum conditions and a case where jet focusing occurs. Data are also presented showing surface erosion produced by the gas shear stresses and data concerning the distances debris is ejected from the erosion craters.

3. RESULTS

Roberts' theory (References 1 and 2) forms the basis for the soil erosion analyses conducted in this study. The governing differential equations are presented and discussed in Appendix A along with a digital computer program listing for effecting their solution. Essentially, Roberts' theory of soil erosion is developed in two parts. The first part consists of a formulation of the forces acting on a soil surface due to the impinging retro-rocket gases. In the second part, a partial differential equation is derived which describes the rate at which soil is eroded from the surface under the action of the surface loads.

Roberts' theory was used first to determine the gas pressure loadings acting on the soil surface and then to determine the soil erosion profiles for variations in the system parameters. Finally, these results in conjunction with the particle trajectory theory presented in Appendix C were used to estimate the range the soil debris would be ejected radially. The results of these computations are presented in this section for the engine and soil parameters listed in Tables 1 and 2.

Table 1. Engine Parameters

Nozzle exit Mach number, M_e	3.98
Nozzle exit radius, r_e (ft)	0.389 \approx 4.67 in
Nozzle exit pressure, p_e (psia)	0.1787
Gas constant, R ($\text{ft}^2/\text{sec}^2 \text{R}$)	2310
Gas specific heat ratio, γ	1.252
Thrust, F (lb)	213
Expansion ratio, ϵ	20
Conical nozzle divergence half angle, (deg)	15
Chamber pressure, p_c (psia)	41.7
Chamber temperature, T_c ($^{\circ}\text{F}$)	5670
Chamber viscosity, μ_c ($\text{lb-sec}/\text{ft}^2$)	1×10^{-6}
Descent rate, V_v (ft/sec)	5

$$d_e = 2,0876 \text{ in}$$

Table 2. Martian Atmospheric and Soil Parameters

Ambient pressure, p_o (psia)	0.0726
Acceleration of gravity, g (ft/sec ²)	12.3
Local surface slope, (deg)	0
Soil particle mass density, σ (slugs/ft ³)	5.81
Soil particle volume concentration, c (percent)	.5 (50.)
Soil internal friction angle, α (deg)	34
Soil particle diameter, D (microns)	10, 50, 300
Soil particle cohesion, τ_{coh} (psf)	1950, 15.5, 0.072

In Table 1, the pseudo chamber pressure was computed from the exit pressure p_e , specific heat ratio γ and mach number M_e from the formula

$$p_c = p_e \left[1 + .5 (\gamma - 1) M_e^2 \right]^{\frac{1}{\gamma - 1}}$$

The soil cohesion values listed in Table 2 were those prescribed by JPL for use in the study. Conservative calculations of erosion were also performed for a cohesionless soil. The values of cohesion of 1950 and 15.5 lb/ft² for the 10 and 50 micron-diameter particles were so large that, theoretically, no soil erosion should occur for soils having the particle diameters listed.

3.1 Surface Loadings

Theoretical surface loading data predicted by the theory in Appendix A (vacuum expansion) are shown in Figures 1 through 4 for nozzle heights of 20, 15, 10 and 5 feet. Figure 1 shows the increment in surface pressure caused by the impinging gases. The figure indicates that the maximum excess surface pressure is .081 psi for a nozzle height of 5 feet. If this pressure is added to the existing ambient pressure of .0726 psi, the pressure would be about .154 psia. The figure indicates that the impinging gas differential pressures are generally less than the ambient pressure; and for all nozzle heights, are less than 10 percent of the ambient pressure at radial distances larger than about 5.5 feet from the stagnation point.

Figure 2 shows the theoretical radial velocity of the gas, u , along the surface for the four nozzle heights. The figure indicates that at the 5 foot

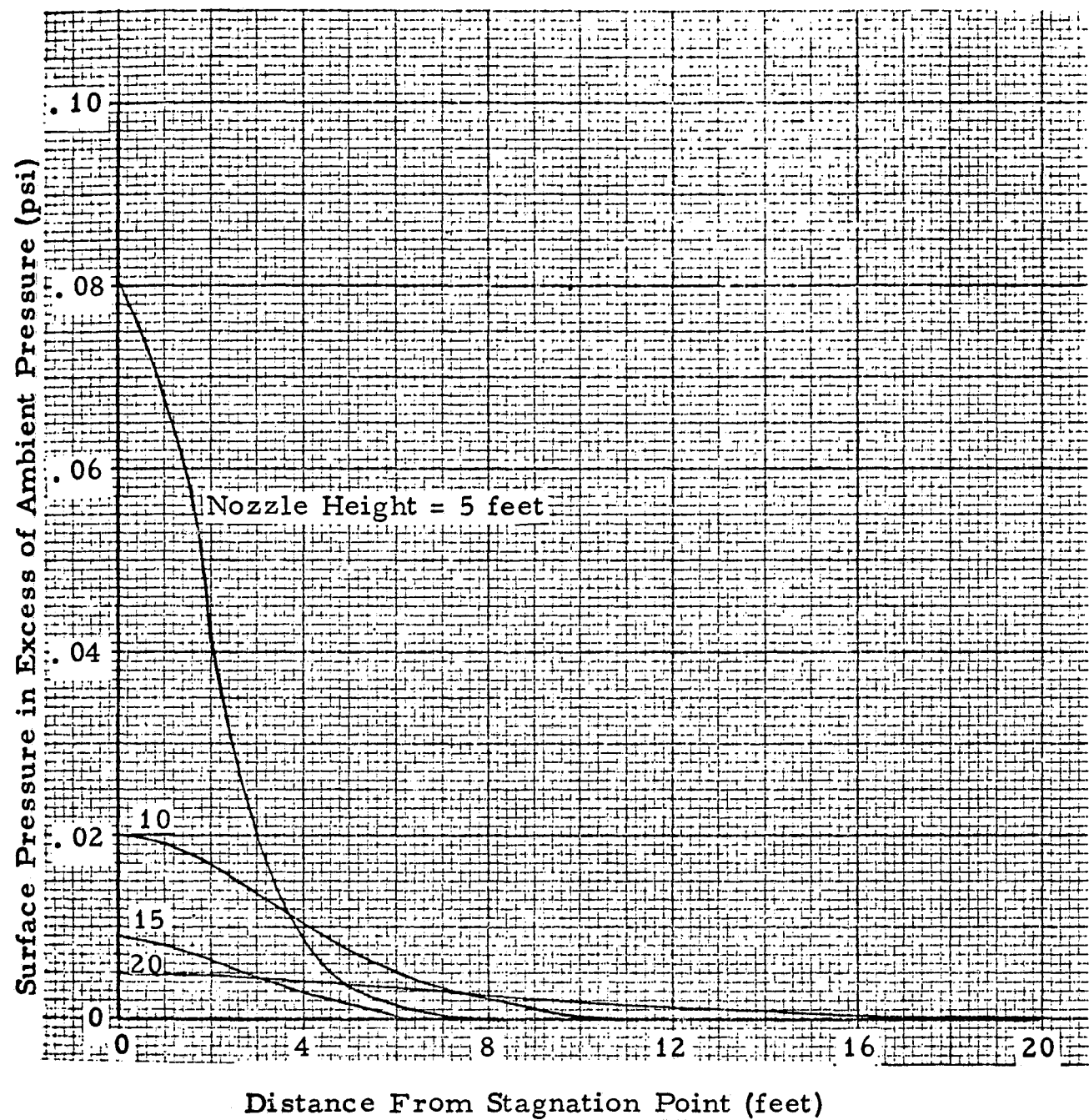


Figure 1. Variations of Surface Pressure With
Nozzle Height (Vacuum Expansion)

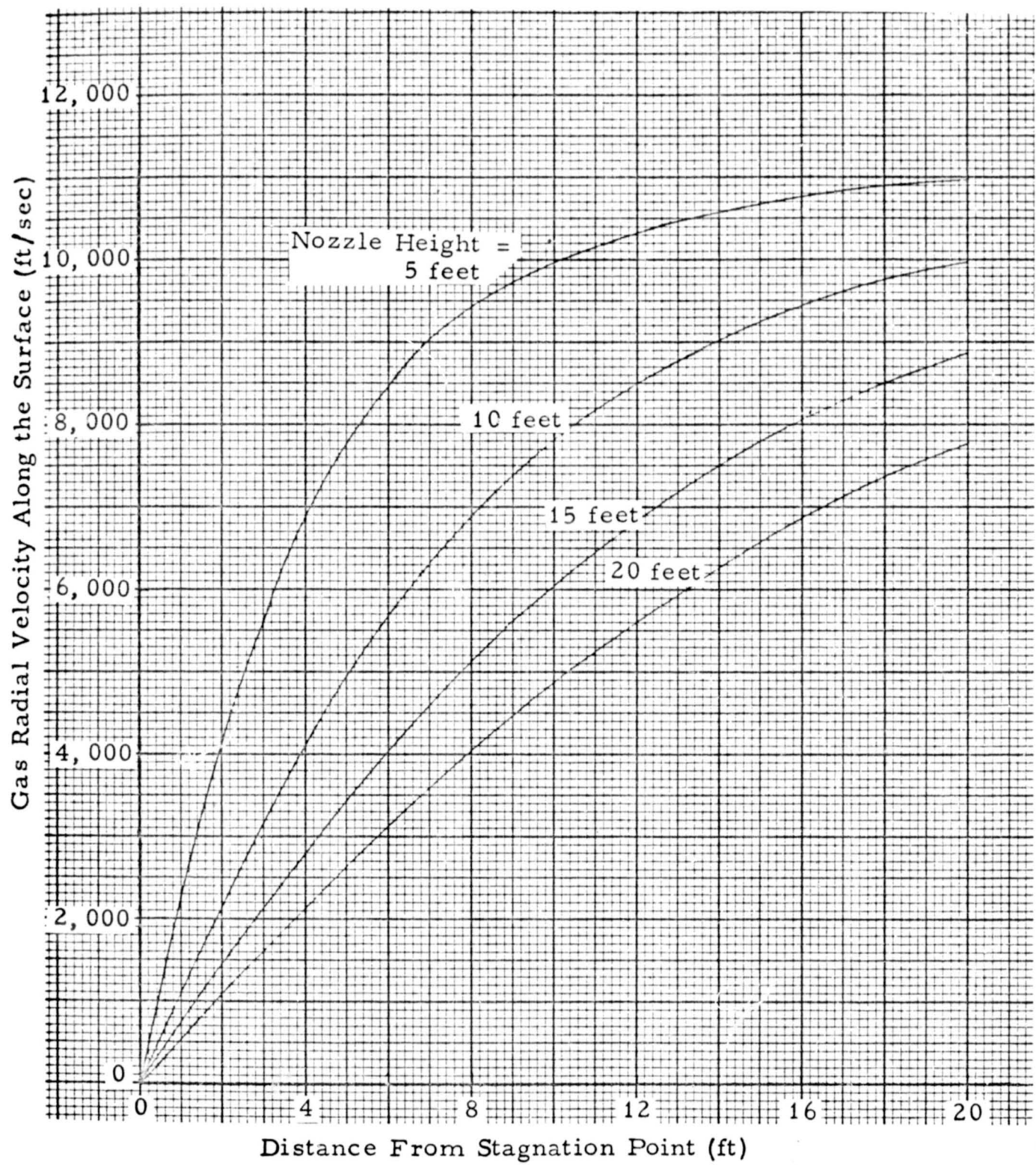


Figure 2. Variation of Gas Radial Velocity Along the Surface With Nozzle Height (Vacuum Expansion)

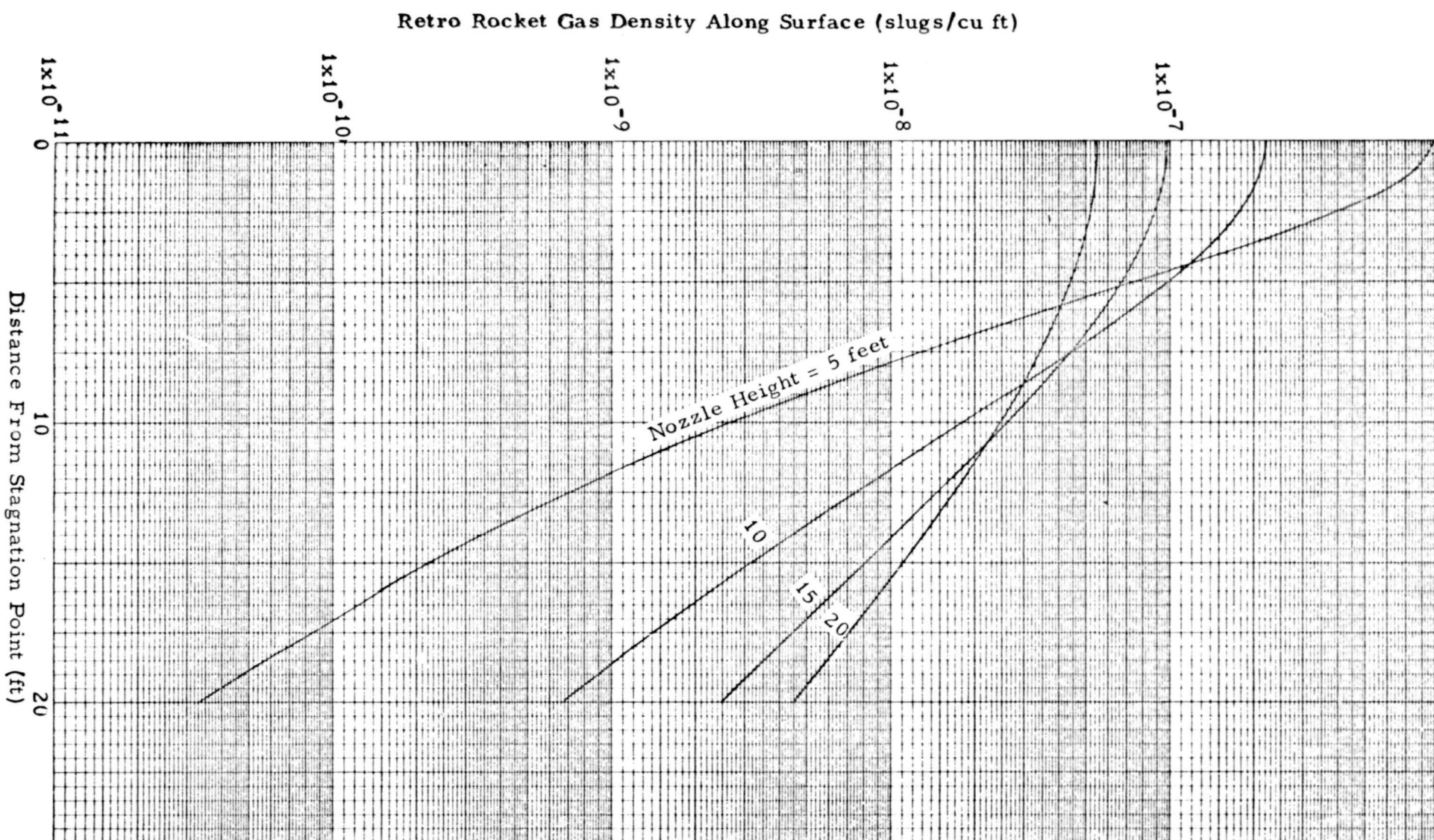


Figure 3. Variation of Retro-Rocket Exhaust Gas Density Along the Surface (Vacuum Expansion)

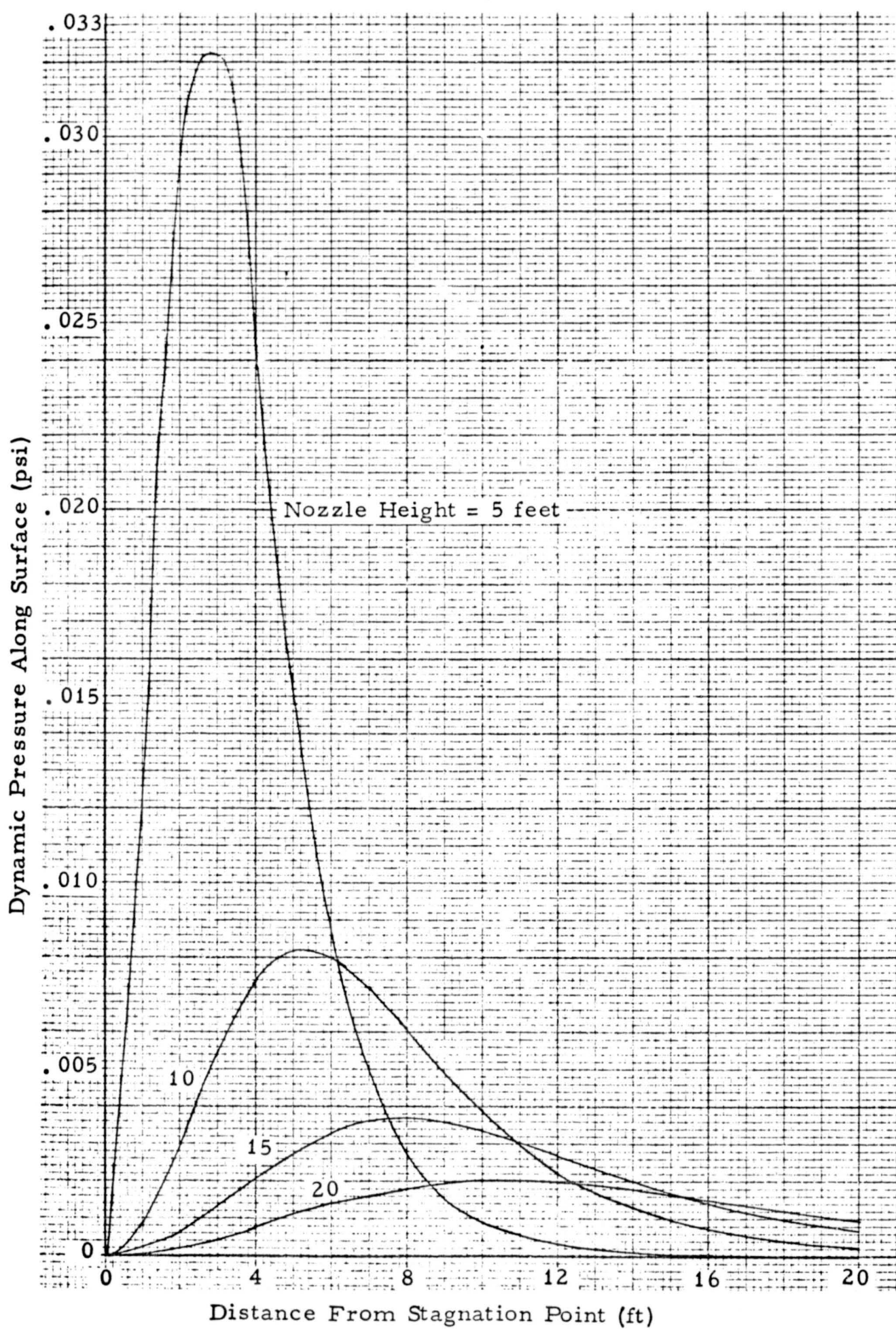


Figure 4. Variation of Dynamic Pressure With
Nozzle Height (Vacuum Expansion)

nozzle height the radial velocity is about 11,000 ft/sec at a distance of 20 feet from the stagnation point. Hence, at this point the gas has almost attained the theoretical velocity of about 11,400 ft/sec to be reached at infinite distances ($p_{\infty} \rightarrow 0$).

Figure 3 shows the exhaust gas mass density ρ along the surface for the four nozzle heights. The figure indicates that the gas density decreases rapidly for increasing distances from the stagnation point.

Figure 4 shows the gas dynamic pressure q (equal to $\rho u^2/2$) along the surface for the four nozzle heights. The viscous shear stress transmitted to the soil is proportional to the dynamic pressure. The figure indicates the maximum dynamic pressure is about .0322 psi (4.64 psf). Thus, for a viscous friction coefficient $C_f = .2$ the maximum shear stress acting on the soil would be about .93 psf. Hence, if the soil restraining stress is greater than .93 psf, theoretically, no soil erosion will occur.

To provide some indication of how the Martian atmosphere may affect surface loadings, calculations were performed for a value of the focusing parameter different from $n = 1$ ($n = 1$ corresponds to expansion into a perfect vacuum). In Appendix B it was found that the jet turning angle was about 114 degrees in a vacuum and 24.6 degrees in a Martian type atmosphere. If one assumes the effective value of the jet focusing parameter n is the square root of the jet turning angles, then $n = 2.15$ and the corresponding surface loadings are as shown in Figures 5 through 8. (The assumption that the jet focusing effect can be accounted for through the single parameter n and its functional dependence on the jet turning angles must, of course, be verified when the necessary test data becomes available.)

A comparison of Figure 1 through 4 with Figures 5 through 8 indicates a value of $n = 2.15$ produces static and dynamic surface pressures about 2.5 times as large as in a perfect vacuum, and the loadings are more concentrated around the stagnation point.

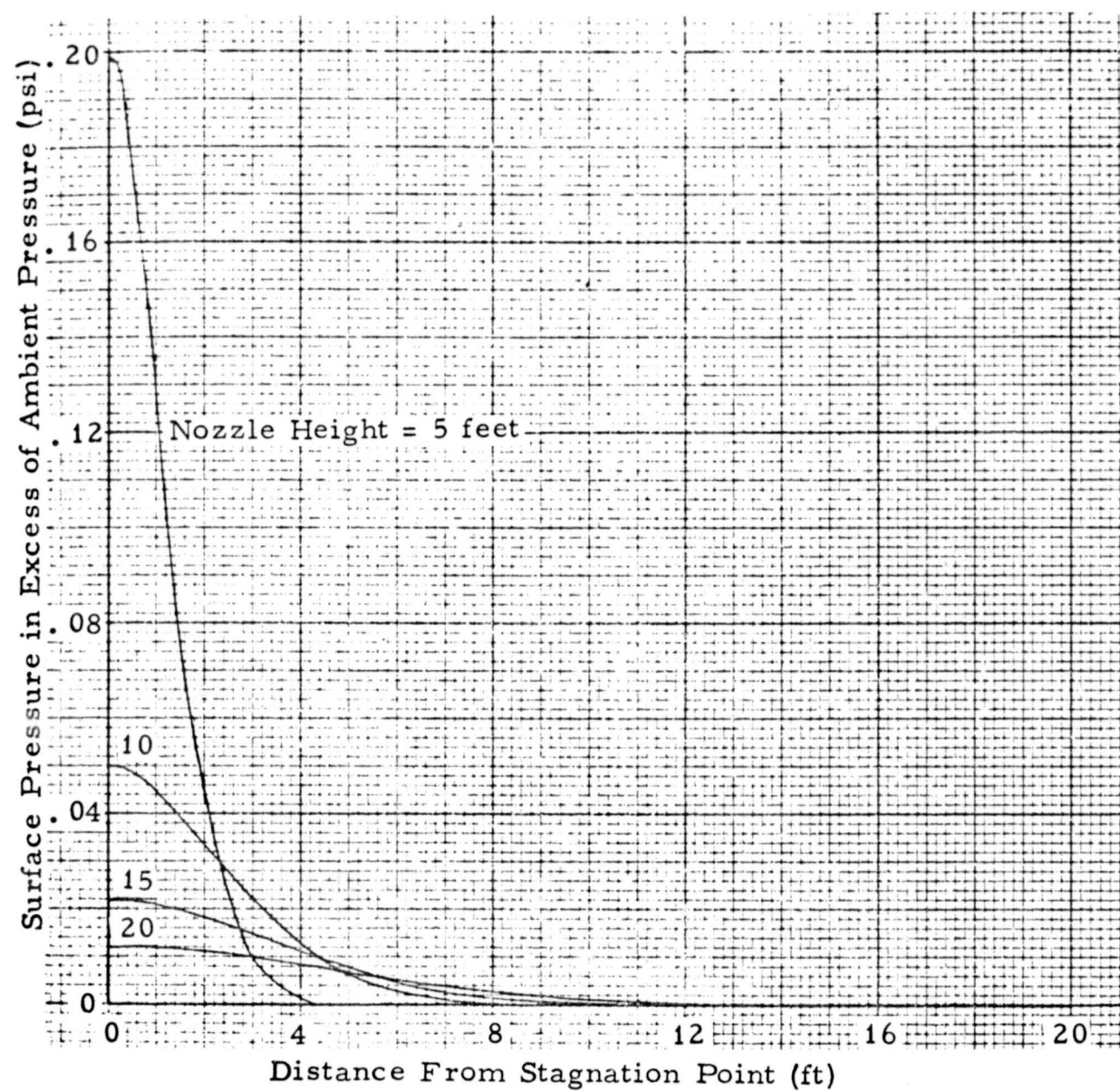


Figure 5. Variation of Surface Pressure
With Nozzle Height
($n = 2.15$)

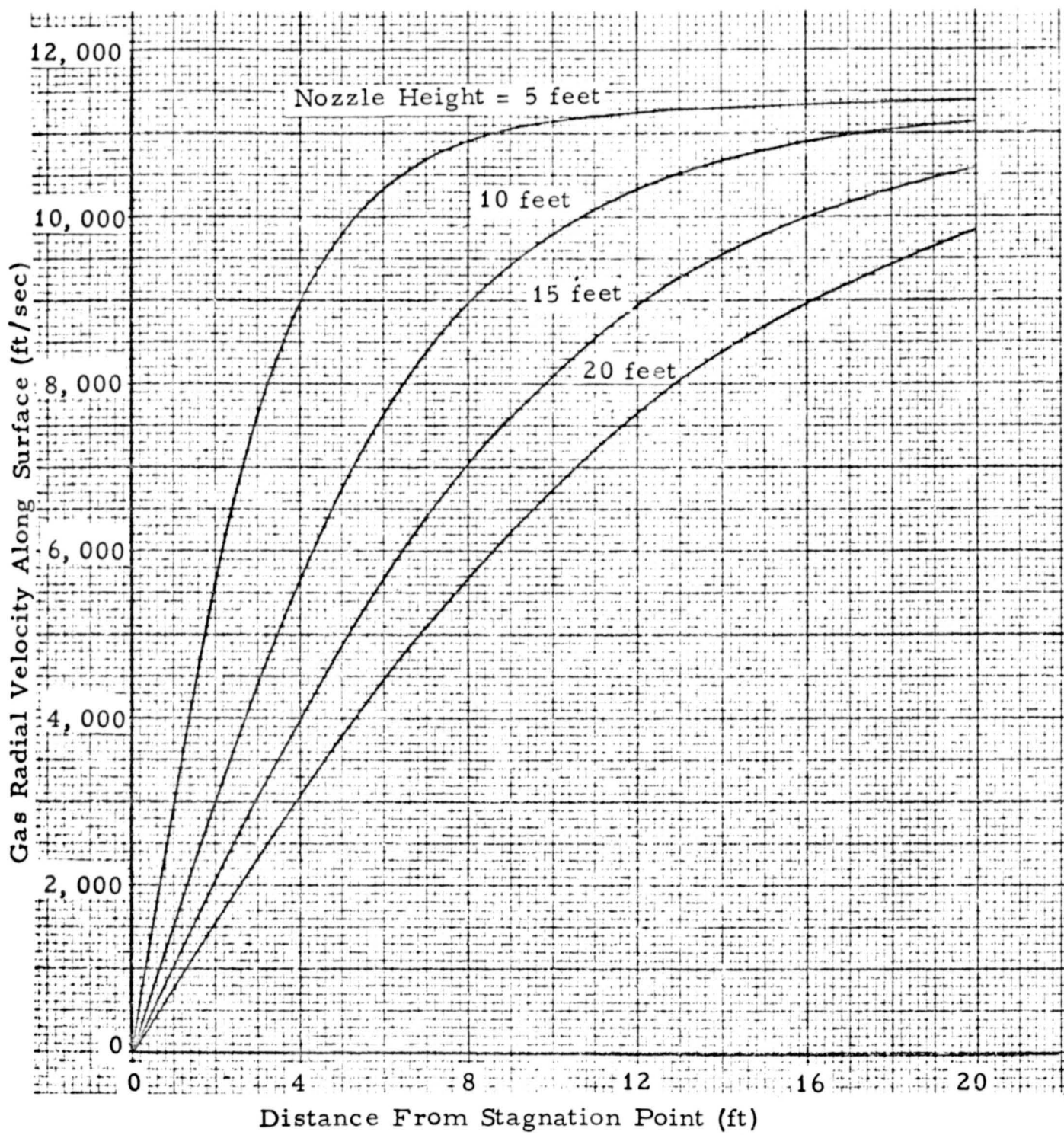


Figure 6. Variation of Gas Radial Velocity Along the Surface With Nozzle Height
($n = 2.15$)

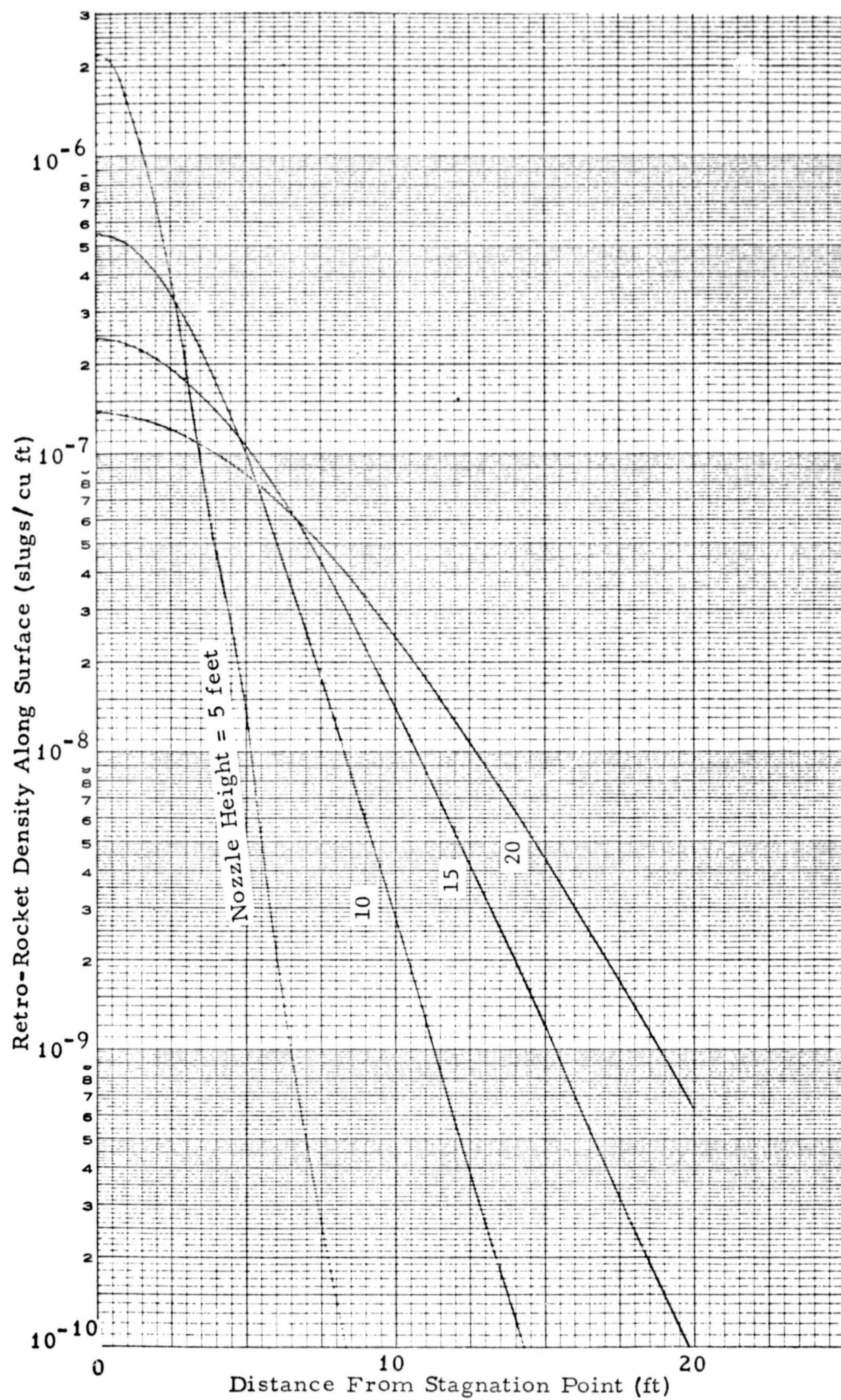


Figure 7. Variation of Retro-Rocket Exhaust Gas Density Along the Surface
($n = 2, 15$)

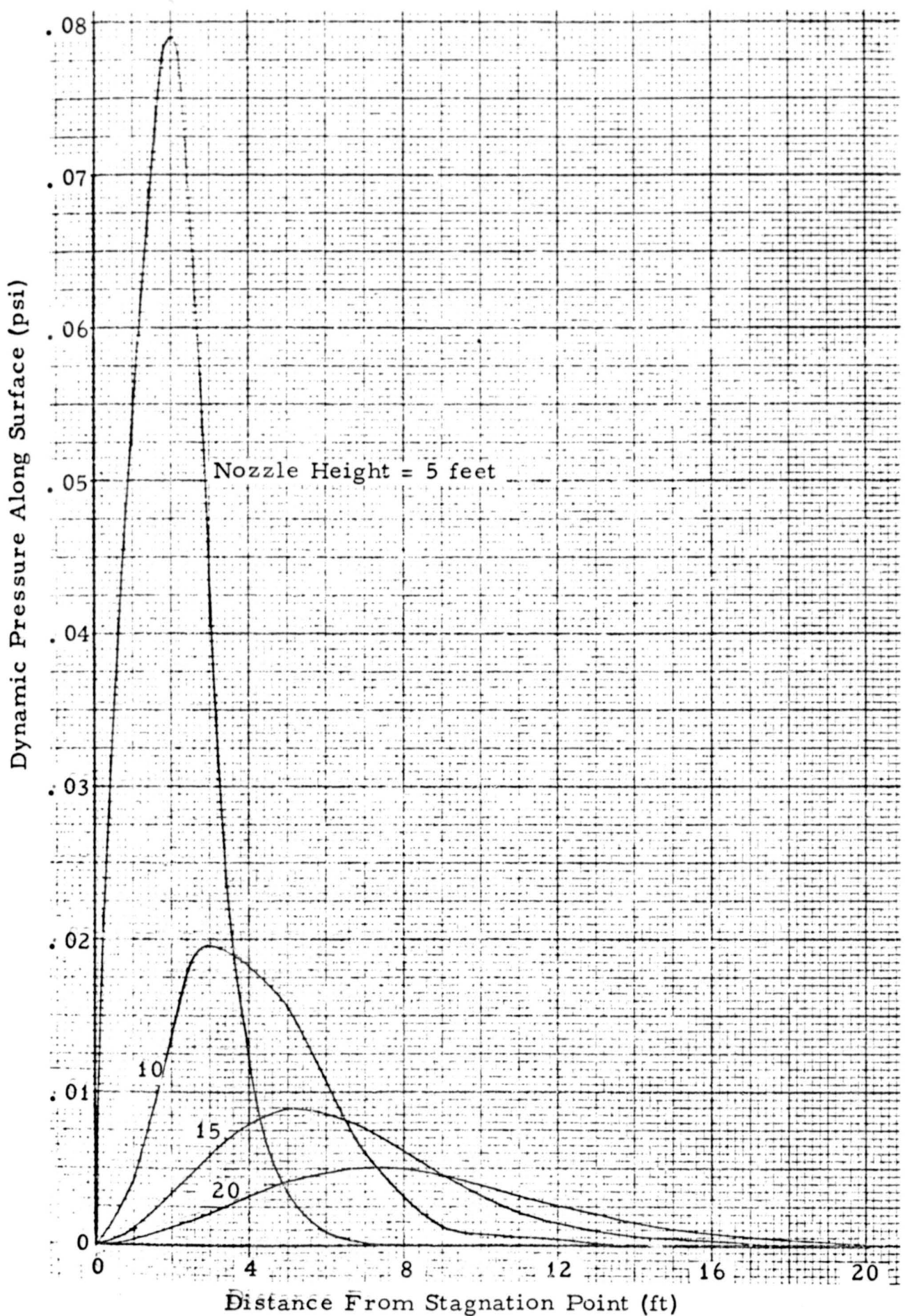


Figure 8. Variation of Dynamic Pressure
With Nozzle Height
($n = 2, 15$)

3.2 Soil Erosion

Theoretical soil erosion data were computed according to the procedure in Appendix A and are presented in this section. Figure 9 shows the soil erosion rate for a range of soil cohesion for three particle diameters when the nozzle is 5 feet above the surface and expanding into a perfect vacuum. The figure indicates that no erosion should occur for any of these particle diameters for a soil cohesion larger than about .93 psf. The shear stress to be exceeded by the gas viscous forces is composed of two parts; soil cohesion and restraint offered by the internal friction. The internal friction restraint on a flat surface is $\sigma CDg \tan \alpha$, which for the 300 micron particles is about 0.021 psf. Thus, in general, this restraint is negligible compared to that offered by the soil cohesion, except in a cohesionless soil. Referring to the soil cohesion values listed in Table 2, one concludes from Figure 5^{9,7} that soil erosion will not occur for the 10 and 50 micron-diameter particles for the 5 foot engine thrust cutoff height, or any higher cutoff height. However, since the listed cohesion values (based upon 0.5 psi for 30μ) may be optimistic, conservative calculations were performed for a cohesionless soil. (For example, lunar soil cohesion estimated from Surveyor data is .02 to .05 psi, or 2.9 to 7.2 psf, for particle diameters less than the resolution of the TV camera of about .01 inch or 25 microns.) The results of these calculations are shown in Figures 10, 11 and 12.

Figure 10 shows the vacuum expansion erosion profiles for 300 micron diameter particles for engine thrust cutoff heights of 20, 15, 10 and 5 feet for a cohesionless soil.

Figure 11 shows the same data for a soil having the cohesion listed in Table 2. Observe that, even for a cohesionless soil, the maximum erosion depth is quite small and is about 0.0017 foot (0.02 inch).

Figures 12 and 13 show the vacuum expansion erosion profiles for 50 and 10 micron diameter particles for a cohesionless soil. Although no erosion should occur for the cohesion values listed in Table 2, even in a cohesionless soil, the erosion is still quite small.

A comment might be made at this point concerning the effect of particle diameter on the shear stress required to produce an erosion and the subsequent rate of erosion. An examination of the theory indicates

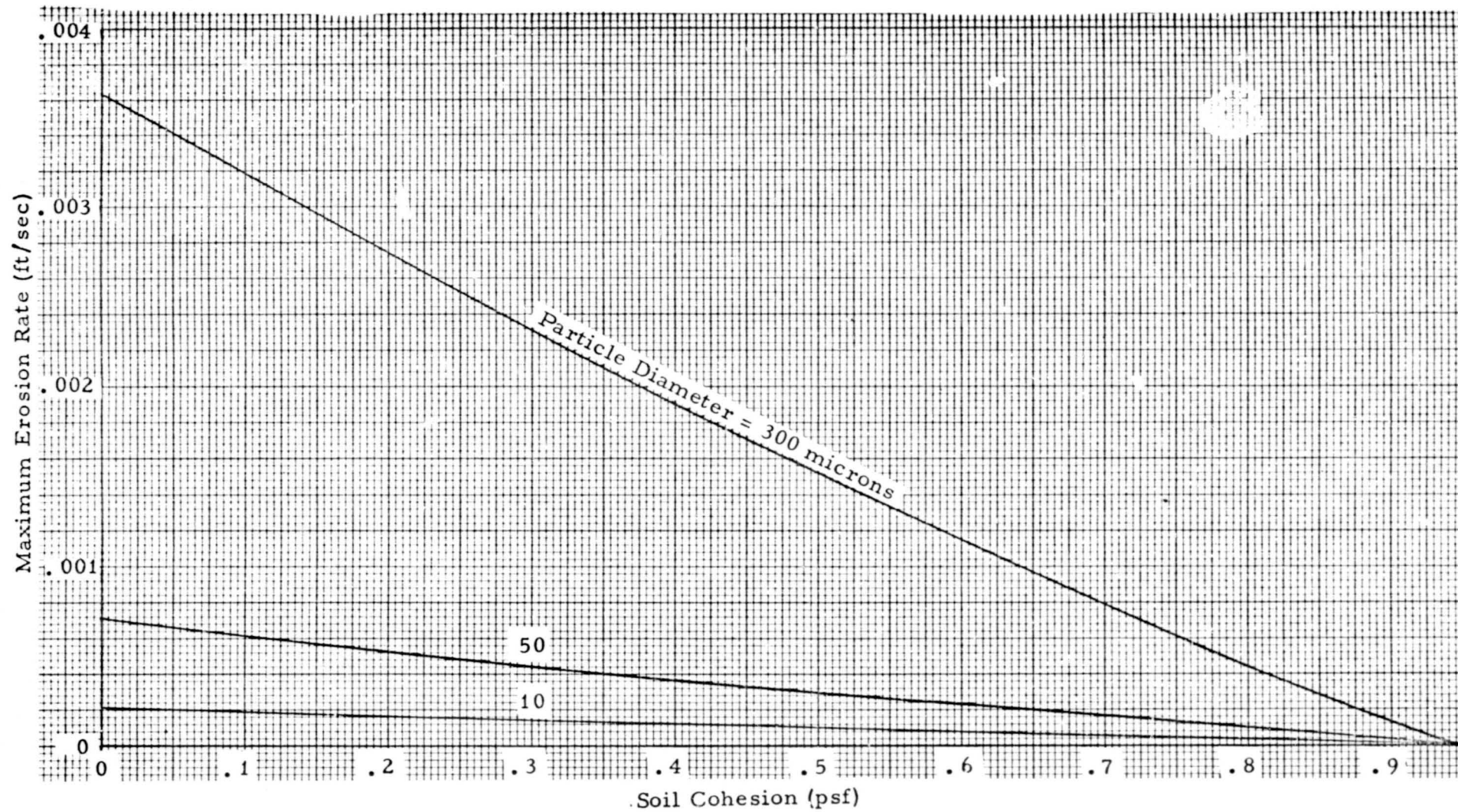


Figure 9. Variation of Maximum Soil Erosion Rate With
Soil Cohesion and Particle Size (Nozzle Height =
5 ft, Vacuum Expansion)

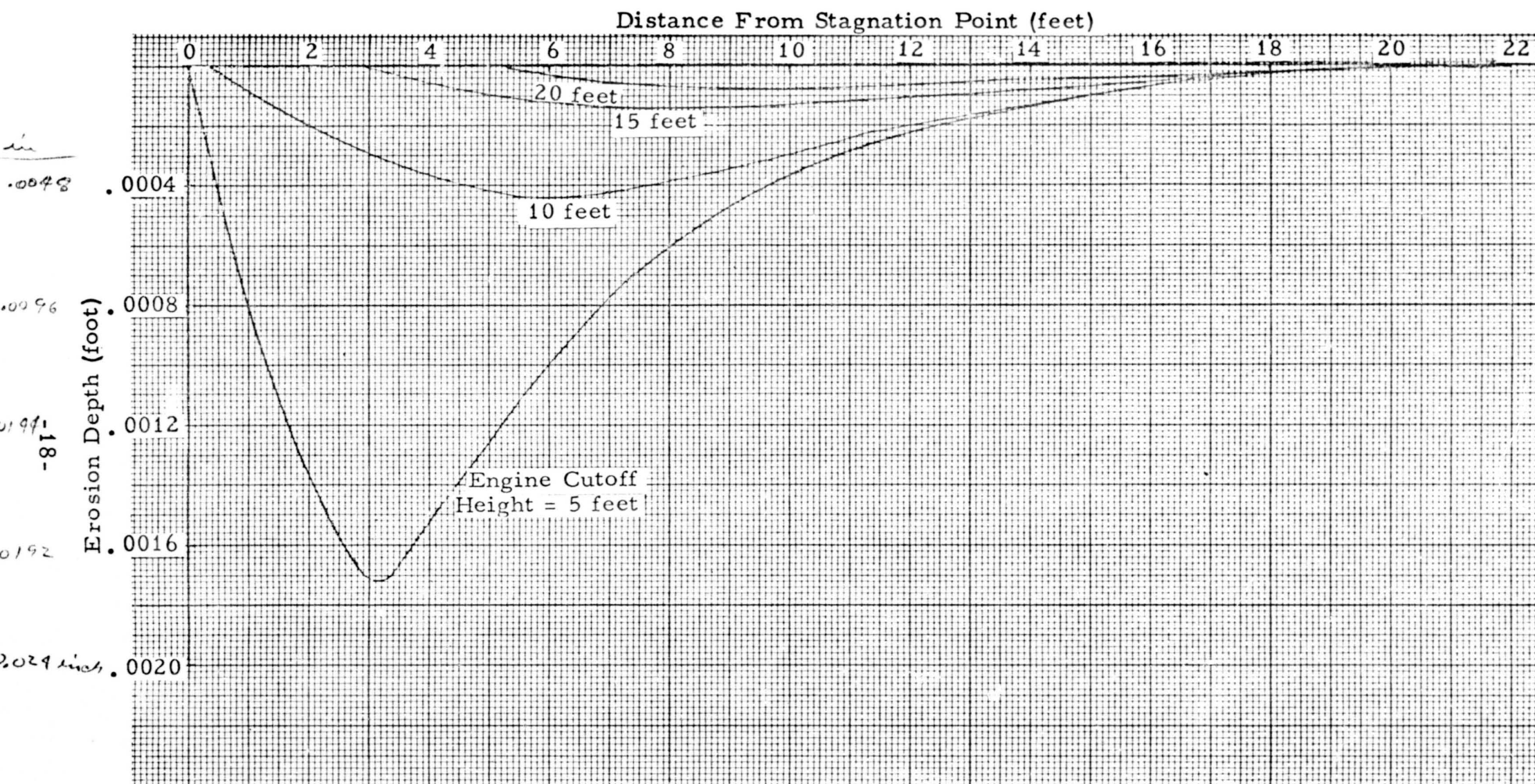


Figure 10. Erosion Profile in a Cohesionless Soil for Various Engine Thrust Cutoff Heights (300 micron diameter soil particles, vacuum expansion)

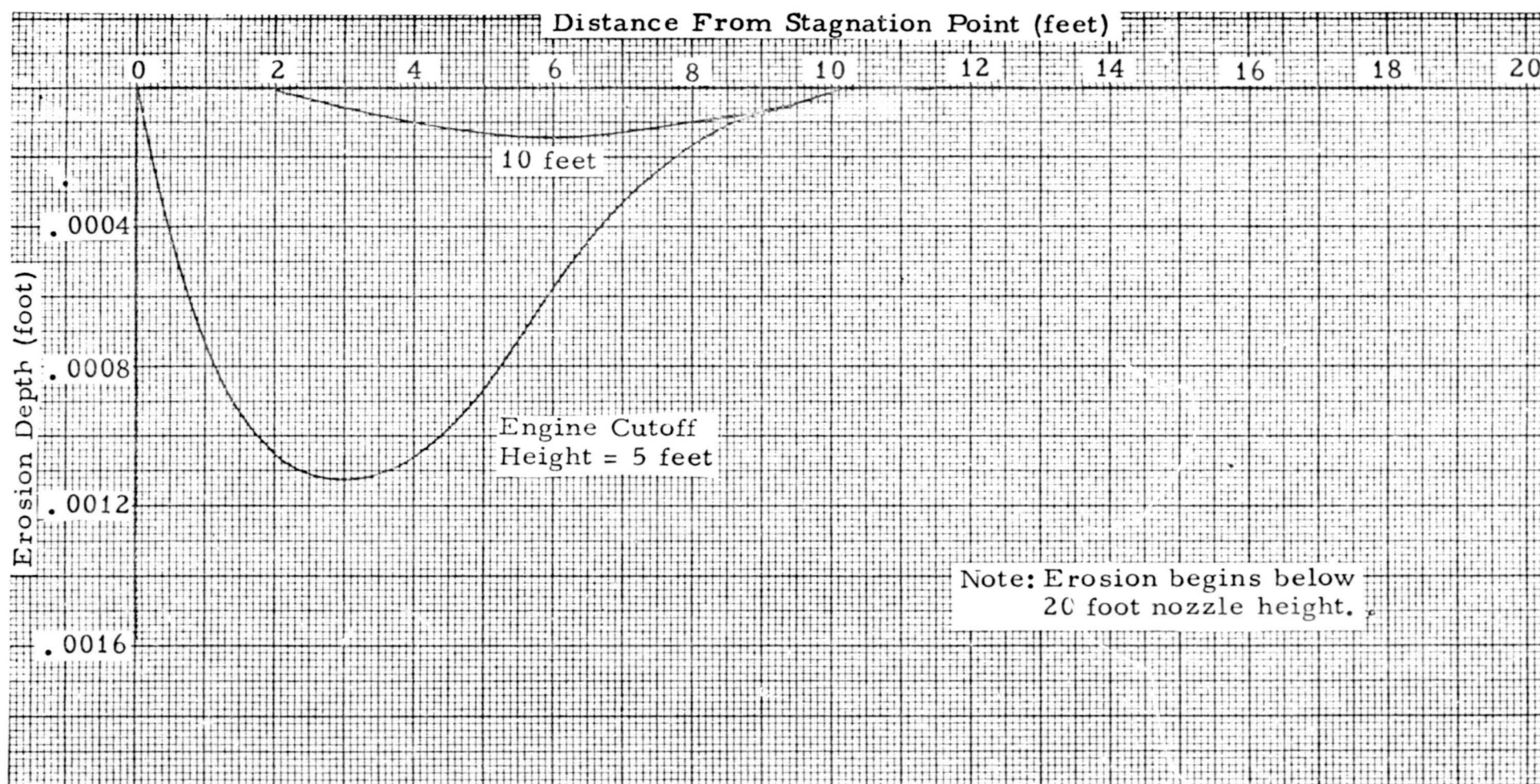


Figure 11. Erosion Profile for Various Engine Thrust Cutoff Heights
(300 micron diameter particles, 0.072 psf cohesion,
vacuum expansion)

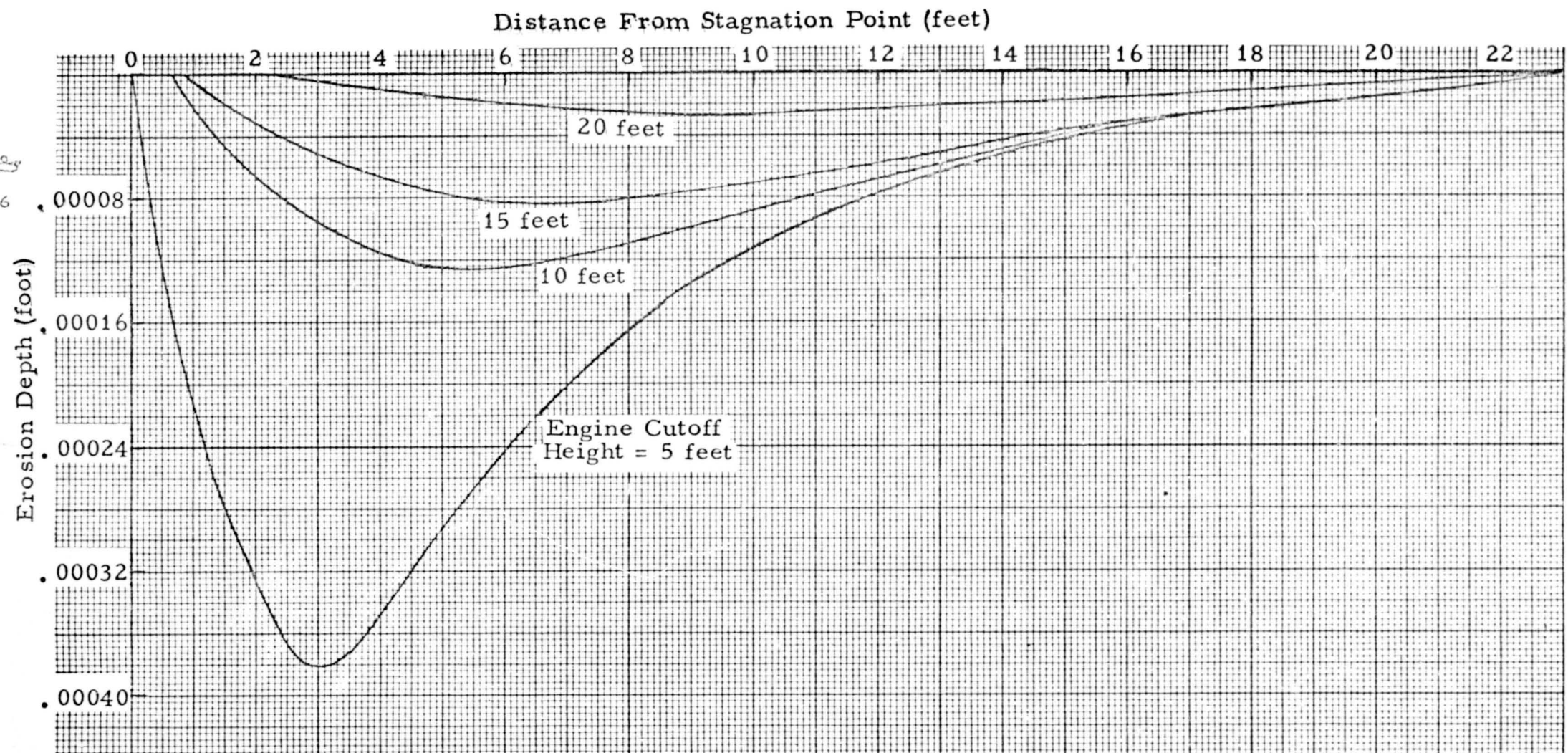


Figure 12. Erosion Profile in a Cohesionless Soil for Various Engine Thrust Cutoff Heights (50 micron diameter soil particles, vacuum expansion)

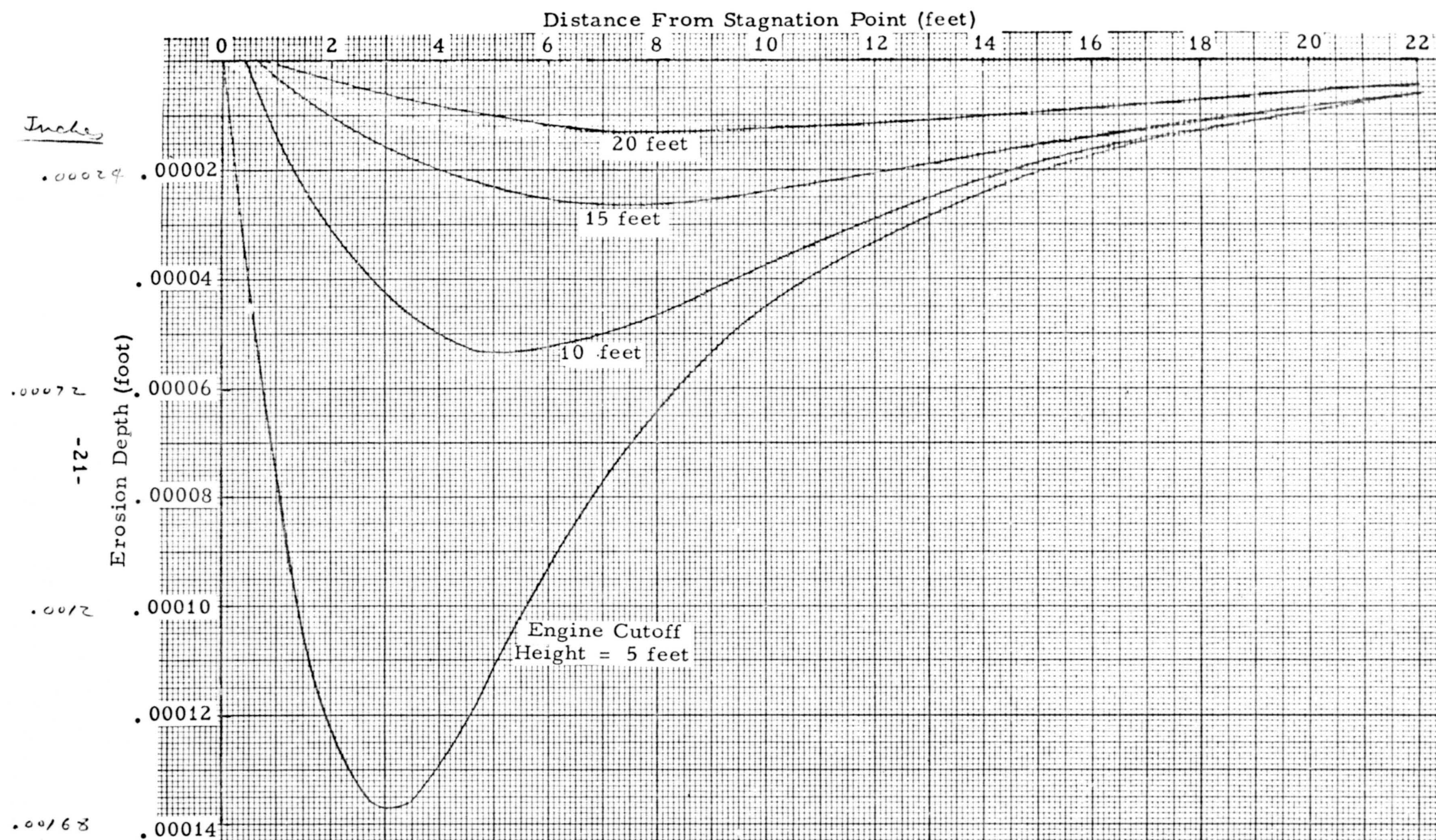


Figure 13. Erosion Profile in a Cohesionless Soil for Various Engine Thrust Cutoff Heights (10 micron diameter soil particles, vacuum expansion)

that for a fixed value of cohesion the shear stress required to produce an erosion is larger for larger diameter particles. This is because the larger the particle, the larger the soil weight; and hence, the larger the restraint offered by the soil as a result of internal friction. However, the differences in restraint are generally negligible compared to any reasonable value of soil cohesion. On the other hand, if the erosive shear stresses are in excess of the restraint offered by the soil, the larger the particle diameter, the larger the rate of erosion. This follows from the fact that the theory is based on a momentum balance between the gas particles and soil particles. Small soil particles are rapidly accelerated and provide an efficient transfer of momentum to the soil, while large soil particles attain only a small fraction of the gas velocity. Soil erosion experiments bear out this behavior and demonstrate that the erosion rate increases with increasing particle diameter until the particles become so large that the frictional restraint exceeds the viscous erosive stresses. To provide some indication of the effect of jet focusing on surface erosion, computations were also performed for the focusing parameter $n = 2.15$. The results are shown in Figures 14 and 15 for a 300 micron-diameter particle soil. The figures show the profiles for a cohesionless soil and a soil having the cohesion listed in Table 2. A comparison of Figure 14 with Figure 10 indicates the maximum erosion depth is about twice that in a perfect vacuum. But even so, it is still quite small.

3.3 Soil Particle Displacements

Because of the very small erosion for the prescribed descent to the Mars surface (even for a cohesionless soil), particles should depart from the surface at very low angles and therefore, have small lateral displacements. The low departure angles are a consequence that, theoretically, the particles leave the surface tangent to the erosion crater. Theory indicates the maximum range is traversed by particles lying between the point of maximum depth and the outer crater lip because the crater slopes are larger in this region. The distance a particle travels from the point it enters the stream depends on the local erosion crater slope and the velocity of the particle. Since a soil composed of a given particle size erodes faster than a surface having smaller particles, the local slope is greater for the larger particles, for the same exposure time to the erosive gas forces. However, the larger particles attain a much smaller

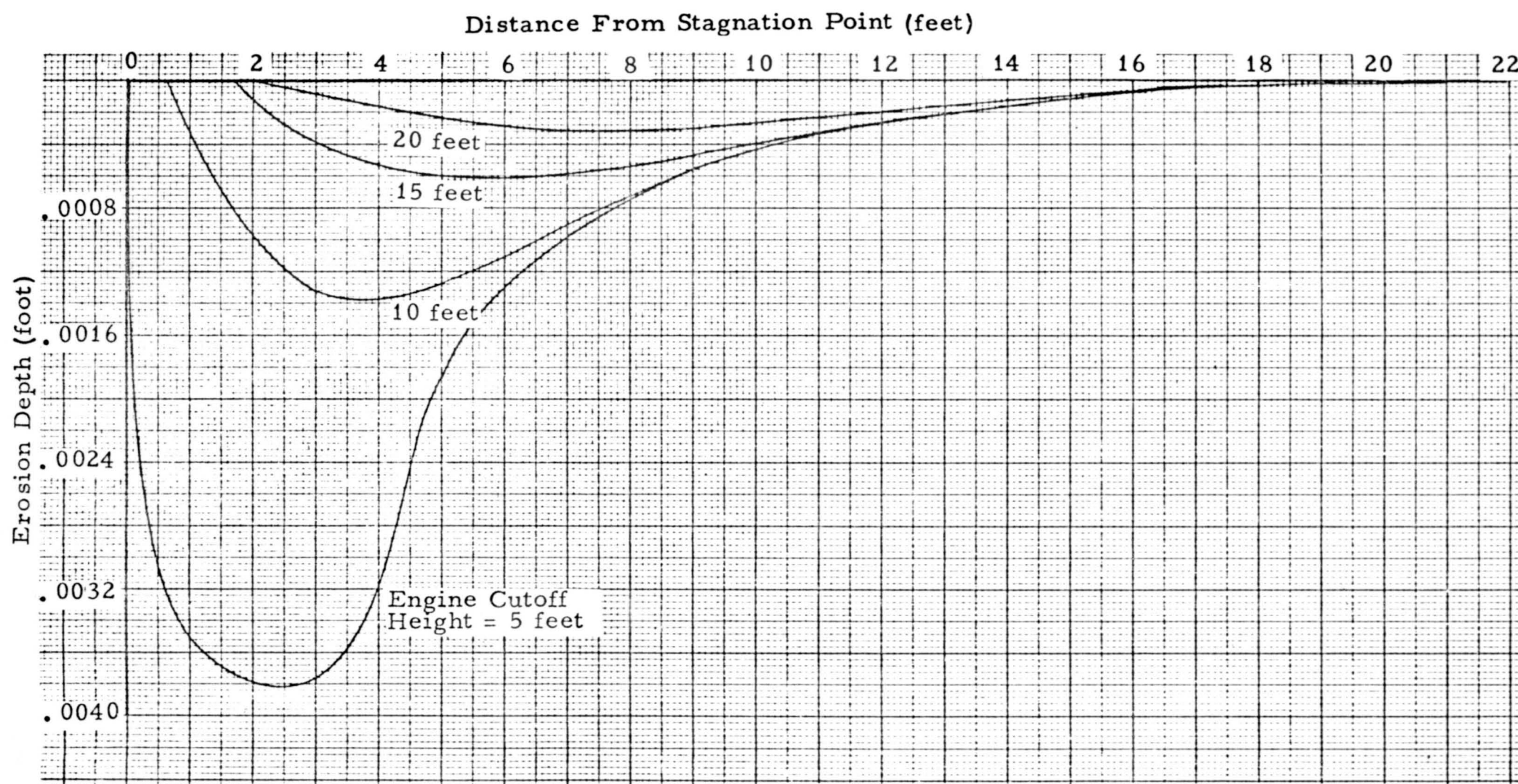


Figure 14. Erosion Profile in a Cohesionless Soil for Various
Engine Thrust Cutoff Heights
(300 micron diameter soil particles)
($n = 2.15$)

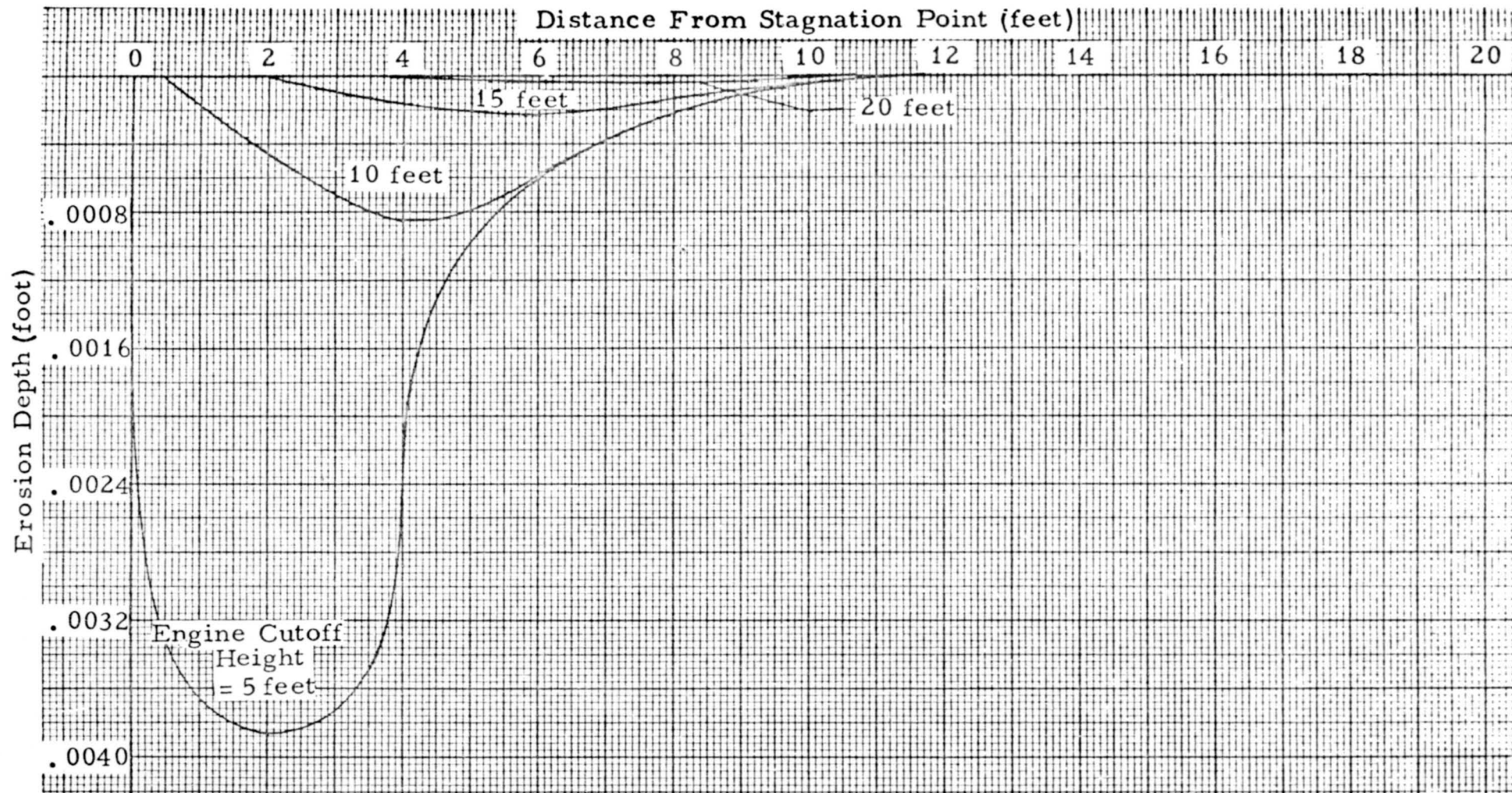


Figure 15. Erosion Profile for Various Engine Thrust Cutoff Heights
(300 micron diameter particles, 0.072 psf cohesion, n = 2.15)

fraction of the gas velocity than the smaller particles. Thus, the ballistic trajectory of larger particles may or may not have a longer range than the range of smaller particles. For the system parameters considered here, along with the 5 foot ^{per second} descent rate, the surface erosion and erosion crater slope are quite small. This results in a relatively small trajectory range for all soil particle diameters considered. Consequently, the surface debris is largely confined to the region in which erosion takes place. As the spacecraft descends toward the surface, the erosion region decreases in size, although erosion rate increases.

In a cohesionless soil, incipient erosion begins around nozzle heights of 170, 80 and 30 feet for the 10, 50 and 300 micron diameter particles, respectively. At these heights, the maximum viscous shearing stresses along the surface are just equal to the restraint offered by the friction between soil grains. At these incipient erosion heights, the points of maximum shear stress are at radial stations located about 93, 42 and 17 feet from the stagnation point for the 10, 50 and 300 micron diameter particles, respectively. Consider, for example, the formation of the erosion crater in a 10 micron diameter cohesionless soil. At the 170 foot nozzle height, a surface erosion begins about 93 feet from the stagnation point. As the spacecraft descends, the region in which erosion takes place moves toward the stagnation point. At engine cutoff, say at a 5 foot nozzle height, the maximum rate of erosion has moved to about 2 feet from the stagnation point. A particle that enters the gas stream just prior to engine cutoff about 7 feet from the stagnation point, where the erosion crater has an upward slope, has a ballistic range in a vacuum of about 90 feet. This range transports the particle approximately to the region where erosion first occurred during descent. Consequently, the distance debris is transported along the surface is essentially confined to the entire region in which erosion takes place during the descent period. As a result, the distance debris is deposited along the surface is essentially the same for 20, 10 or 5 foot engine thrust cutoff heights. An exception is provided by 100 micron particles for a 5 foot nozzle cutoff height. In this case, the erosion is fast enough to produce a local slope such that the ballistic trajectory of a particle located about 8 feet from the stagnation point travels about 10 feet beyond the incipient erosion point.

Results of soil particle displacements computations are summarized in Figure 16. The particle velocities and departure angles used in the calculations were those obtained from the erosion calculations. These were compared with the limiting erosion profile also obtained from the same calculations. The range plotted is the larger of these two results, which, as indicated earlier, generally was the limit of the erosion crater. It should be recalled that, if the soil cohesion is as large as listed in Table 2, no erosion of particles smaller than 50 microns in diameter should occur. Therefore, the particle displacement ranges shown for particle diameters up to 50 microns should be an extreme upper bound estimate.

Even though this theory indicates the erosion should be small and the particles displaced only small distances, one should not overlook the idealization of the theory. For example, an actual soil surface is most likely undulating, nonhomogeneous and composed of a distribution of particle sizes. The variations in local slope of the virgin surface most likely exceeds the maximum slope predicted here for the erosion crater. Hence, soil particles may depart from the surface with velocities comparable to those predicted here, but at angles larger than the crater profile makes with the horizontal. It seems quite likely they could depart from the surface at angles as large as 15 degrees. In such an event, the theory in Appendix C would predict the ranges tabulated in Table 3.

Table 3. Theoretical Range for 5 Foot Engine Cutoff Height and 15 Degree Departure Angle

Soil Particle Diameter (microns)	Soil Particle Velocity (ft/sec)	Range (ft)	
		Vacuum	Atmosphere ($C_D = 0.14$)
10	6011	1,470,000	194
50	1861	141,000	675
300	350	4,964	1420

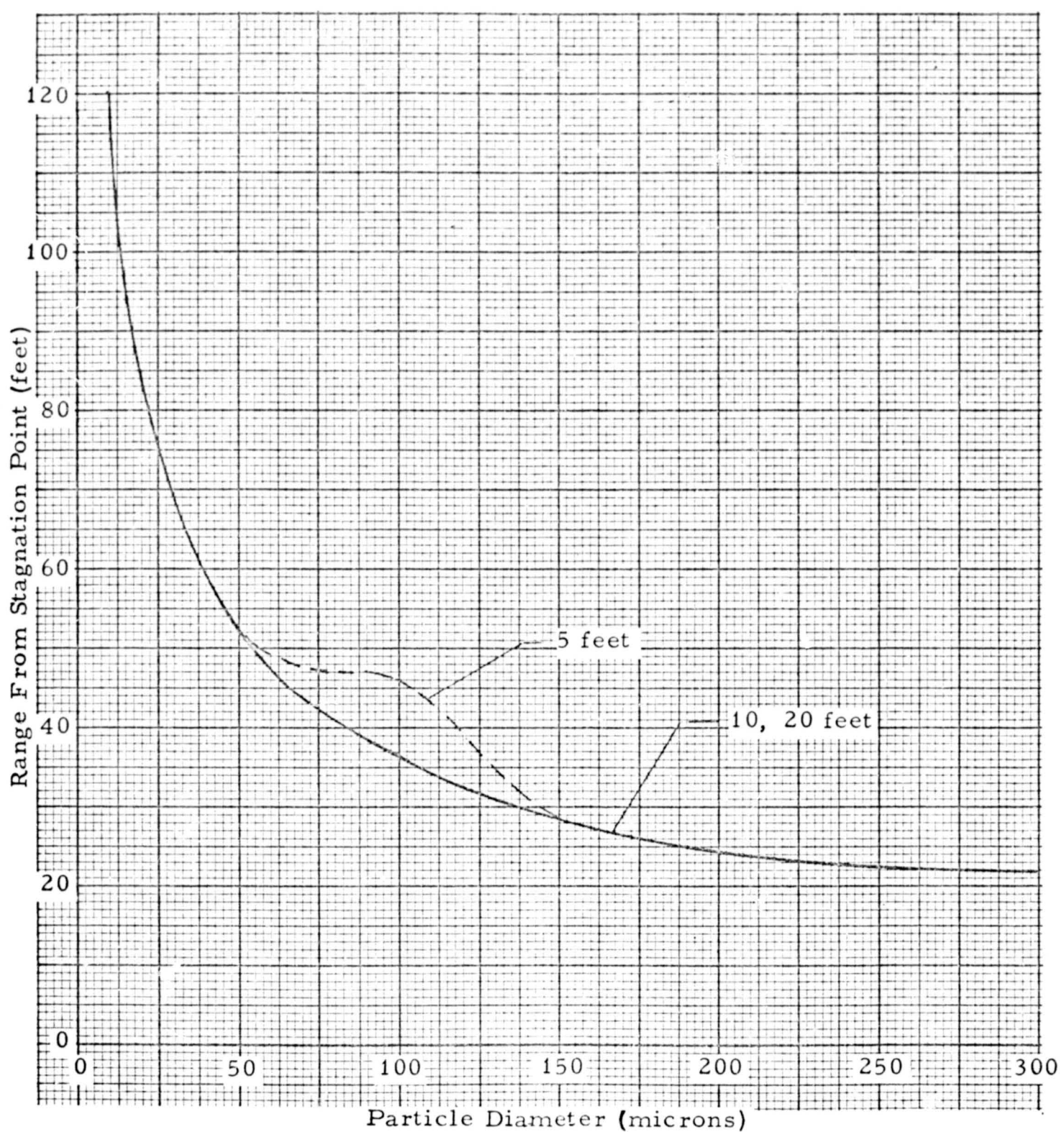


Figure 16. Variation of Debris Impact Point With Particle Diameter and Engine Thrust Cutoff Height (cohesionless soil)

These data were based on drag coefficients of 0 and 0.14 corresponding to vacuum and atmospheric conditions. The density of the Martian atmosphere used in these calculations was estimated from the ambient pressure of 0.0726 psi (10.45 psf). The estimate was made based on CO₂ whose molecular weight is 44 and at a temperature of 128°R. The gas constant and density were then computed to be

$$R = \frac{49686}{44} = 1130 \text{ ft}^2/\text{sec}^2 \text{ °R}$$

$$\rho = \frac{P}{RT} = \frac{10.45}{(1130)(128)} = 7.22 \times 10^{-5} \text{ slugs/ft}^3$$

These values indicate the range could far exceed those shown in Figure 16. The tabulated results in Table 3 reflect the fact that small-diameter particles are readily accelerated by the gas stream, and the subsequent ballistic trajectory in a vacuum would have an extremely large range. However, these same small particles would be readily decelerated by the drag forces produced by the Martian atmosphere. It should be emphasized that the ranges computed for atmospheric conditions are the result of certain basic assumptions. First, it assumes the retarding aerodynamic force is proportional to the square of the particle velocity. This seems reasonable, but may only be valid over a limited portion of the entire velocity range. Second, even if the velocity square drag law is valid, the corresponding drag coefficient may vary with particle diameter and velocity (or Reynolds number). If this is the case, the estimated value of C_D = 0.14 from bullet range data, which have diameters much larger than the soil particles, may be in error. If the drag coefficient was significantly smaller than the value used here, the ranges in the presence of an atmosphere would approach that in a vacuum condition.

In summary, erosion calculations indicate surface erosion to be negligible for the range of parameters considered in this study, even for a cohesionless Martian soil. The corresponding range debris is displaced laterally along the surface should be less than 30 feet from the stagnation point, but may be as large as 120 feet if the soil is cohesionless. On the other hand, one cannot rule out the possibility that the local surface roughness may cause some particles to be displaced to larger distances. The

These data were based on drag coefficients of 0 and 0.14 corresponding to vacuum and atmospheric conditions. The density of the Martian atmosphere used in these calculations was estimated from the ambient pressure of 0.0726 psi (10.45 psf). The estimate was made based on CO₂ whose molecular weight is 44 and at a temperature of 128°R. The gas constant and density were then computed to be

$$R = \frac{49686}{44} = 1130 \text{ ft}^2/\text{sec}^2 \text{ °R}$$

$$\rho = \frac{P}{RT} = \frac{10.45}{(1130)(128)} = 7.22 \times 10^{-5} \text{ slugs/ft}^3$$

These values indicate the range could far exceed those shown in Figure 16. The tabulated results in Table 3 reflect the fact that small-diameter particles are readily accelerated by the gas stream, and the subsequent ballistic trajectory in a vacuum would have an extremely large range. However, these same small particles would be readily decelerated by the drag forces produced by the Martian atmosphere. It should be emphasized that the ranges computed for atmospheric conditions are the result of certain basic assumptions. First, it assumes the retarding aerodynamic force is proportional to the square of the particle velocity. This seems reasonable, but may only be valid over a limited portion of the entire velocity range. Second, even if the velocity square drag law is valid, the corresponding drag coefficient may vary with particle diameter and velocity (or Reynolds number). If this is the case, the estimated value of C_D = 0.14 from bullet range data, which have diameters much larger than the soil particles, may be in error. If the drag coefficient was significantly smaller than the value used here, the ranges in the presence of an atmosphere would approach that in a vacuum condition.

In summary, erosion calculations indicate surface erosion to be negligible for the range of parameters considered in this study, even for a cohesionless Martian soil. The corresponding range debris is displaced laterally along the surface should be less than 30 feet from the stagnation point, but may be as large as 120 feet if the soil is cohesionless. On the other hand, one cannot rule out the possibility that the local surface roughness may cause some particles to be displaced to larger distances. The

possibility exists, although most likely quite remote, that some particles could have ranges as large as, or larger than, 1400 feet from the stagnation point.

REFERENCES

1. Leonard Roberts, "The Action of a Hypersonic Jet on a Dust Layer," Presented at the Thirty-First Annual Meeting of the Institute of the Aerospace Sciences, January 1963.
2. Leonard Roberts, "The Interaction of a Rocket Exhaust with the Lunar Surface," Presented at a Specialists' Meeting on Fluid Dynamic Aspects of Space Flight, under the Sponsorship of the Fluid Dynamics Panel of the Advisory Group for Aeronautical Research and Development, Marseilles, France, April 20-24, 1964.
3. R. E. Hutton, "An Investigation of Soil Erosion and Its Potential Hazard to LM Lunar Landing," Prepared for the National Aeronautics and Space Administration, Manned Spacecraft Center, Houston, Texas, TRW Systems Engineering Mechanics Report EM 16-11, October 1966.
4. E. K. Latvala, "Spreading of Rocket Exhaust Jets at High Altitudes," AEDC-TR-59-11, June 1959.
5. H. W. Liepmann, A. Roshko, Elements of Gasdynamics, John Wiley & Sons, New York, 1960.
6. J. S. Hatcher, Hatcher's Notebook, Stackpole Company, Harrisburg, Pennsylvania, 1947.

APPENDIX A. ROBERTS' THEORY

In References 1 and 2 Roberts first develops a description of the gas flow field caused by the gases emanating from a nozzle located a distance h above a flat soil surface. He then develops a theory describing the rate the soil surface erodes under the action of the gas viscous forces generated while the gas flows from the stagnation point radially outward along the soil surface.

Initially, Roberts make an assumption regarding the spatial variation in gas density as it emanates from the nozzle. Then, by applying perfect gas theory and boundary layer theory, analytical expressions are developed to describe the gas radial velocity, static and dynamic pressures along the soil surface, and viscous shear forces acting on the soil. An impulse-momentum relation is then postulated to exist in the form

$$(\Delta m) v = A (\tau - \tau^*) \Delta t \quad (A1)$$

which relates the momentum change of soil mass Δm to the impulse caused by the gas viscous shear forces. In Equation (A1), v is the velocity imparted to the element of soil mass, A is the cross-sectional area of the element of mass, τ is the viscous shear stress acting on the soil mass, and τ^* is the soil restraining shear force due to friction and cohesion between the soil grains that must be exceeded before erosion can begin. The coordinate system used in this derivation is shown in Figure A1.

The element of soil mass and its velocity is then written as

$$\begin{aligned} \Delta m &= \sigma c A \Delta y \cos \beta \\ v &= au/2 \end{aligned} \quad (A2)$$

where σc is the soil bulk mass density (c is the packing factor which is also equal to 1 minus the soil porosity), Δy is the element of erosion depth, β is the slope of the surface, u is the radial velocity of the gas, and $(a/2)$ is the effective proportion of the gas velocity imparted to the soil particle. By taking the proper limit, the partial differential equation describing the rate of erosion is finally obtained. The system of equations developed by Roberts, with some modifications made in Reference 3, is

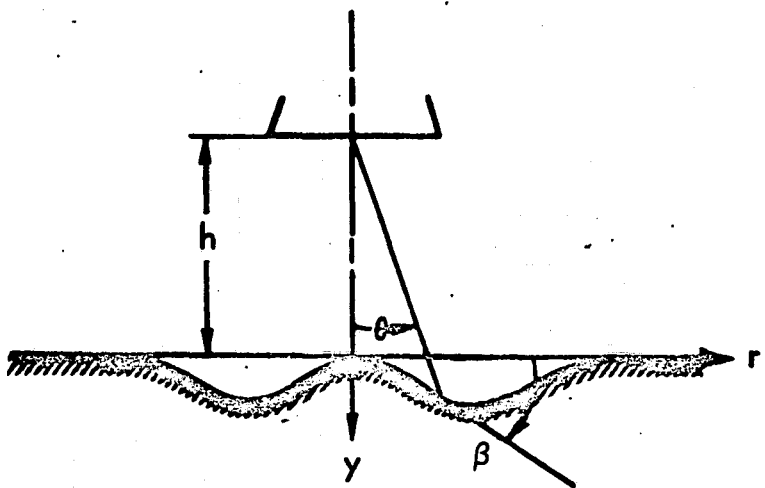


Figure A1. Coordinate System

presented following the definition of symbols. The modifications made in Reference 3 are discussed briefly following the equations.

1. Definition of Symbols

Engine Parameters

- γ = gas specific heat ratio (dimensionless)
 M_e = Mach no. at exit (dimensionless)
 r_e = nozzle exit radius (ft)
 R = gas constant ($\text{ft}^2/\text{sec}^2 \text{ }^\circ\text{R}$)
 T_c = chamber gas temperature ($^\circ\text{R}$)
 μ_c = chamber gas viscosity ($\text{lb-sec}/\text{ft}^2$)
 p_c = chamber gas pressure (psf)
 k = engine parameter (dimensionless)

Flow Field Parameters

- p_r = recovery pressure (psf)
 p_s = stagnation pressure (psf)
 p = surface pressure (psf)
 q = dynamic pressure based on gas radial velocity u (psf)
 u = gas radial velocity along the surface (ft/sec)
 ρ = gas mass density (slugs/ ft^3)
 τ = shear stress acting on soil (psf) = $q C_f$ (for rough turbulent flow)
 C_f = shear stress coefficient (dimensionless)

Soil Parameters

- a = ratio of soil particle velocity to gas velocity (dimensionless)
 D = soil particle size (ft)
 σ = soil mass density (slugs/ ft^3)
 c = soil packing constant [=1 minus porosity, (dimensionless)]
 A_{coh} = cohesion parameter (Roberts recommends 5×10^{-17} lb-ft; used 7×10^{-11} based upon $F_{coh} = 0.5$ psi for 30μ particle size)
 τ_{coh} = soil cohesive stress (lb/ft^2)

Soil Parameters

- α = soil internal friction angle (radians)
 τ^* = soil restraining shear stress (psf)
 v = velocity of soil particle entrained in the flow (ft/sec)

Miscellaneous Parameters

- A = cross sectional area of soil element (ft^2)
 a_0, a_1 = parameter in friction coefficient equation (dimensionless)
 a_2 = parameter in h equation $\approx .25$ (dimensionless)
 a_3 = parameter in R_1 equation $\approx .5$ (dimensionless)
 C_D = particle drag coefficient (dimensionless)
 F = approximate engine thrust (lb)
 g = acceleration of gravity (ft/sec^2)
 h = height of nozzle exit plane (ft)
 h_0 = nozzle height at time $t = 0$ (ft)
 h_1 = nozzle height at hover (engine cutoff) (ft)
 n = jet gas plume focusing parameter ($n=1$ in perfect vacuum, dimensionless)
 r = radial station measured from stagnation point (ft)
 R_1 = radial parameter \approx point at maximum viscous shear stress (ft)
 t = time (sec)
 t_1 = time at which hover/cutoff begins (sec)
 T = final time (sec)
 V_v = vertical descent rate (ft/sec)
 y = soil erosion depth (ft)
 y_{\max} = maximum value of y (along r) at each time increment (ft)
 \dot{y} = soil erosion rate (ft/sec)
 β = slope of erosion crater $\partial y / \partial r$ (radians)
 ζ = parameter in equation for "a" (dimensionless)

2. Governing Equations

Erosion Equation

$$\frac{\partial y}{\partial t} = \frac{2(\tau - \tau^*)}{au \sigma c \cos \beta} \quad (A3)$$

Flow Field Equations

$$u = \left\{ \frac{2\gamma}{\gamma-1} RT_c \left[1 - \left(\frac{p}{p_s} \right)^{\frac{\gamma-1}{\gamma}} \right] \right\}^{\frac{1}{2}} \quad (A4)$$

$$q = \frac{\gamma}{\gamma-1} \left[1 - \left(\frac{p}{p_s} \right)^{\frac{\gamma-1}{\gamma}} \right] \left(\frac{p}{p_s} \right)^{\frac{1}{\gamma}} p_s \quad (A5)$$

$$\frac{p}{p_s} = (\cos \theta)^{n(k+4)} (\cos \beta)^2 [1 - \tan \theta \tan \beta]^2 \quad (A6)$$

$$\rho = \frac{2q}{u^2} \quad (A7)$$

$$\tan \theta = \frac{r}{h}, \tan \beta = \frac{\partial y}{\partial r} \quad (A8)$$

$$p_s = \min \left\{ \frac{p_r}{\frac{n(k+4)-2}{2} \left(\frac{r_e}{h} \right)^2}, p_r \right\} \quad (A9)$$

$$p_r = \frac{\left[1 + \gamma M_e^2 \right] p_c}{\left[1 + \frac{\gamma-1}{2} M_e^2 \right]^{\frac{\gamma}{\gamma-1}}} \quad (A10)$$

$$k = \gamma(\gamma-1) M_e^2 \quad (A11)$$

$$h(t) = h_1(t) + a_2 y_{\max}(t) \quad (A12)$$

$$h_1(t) = \begin{cases} h_o - V_v t & 0 \leq t \leq t_1 \\ h_o - V_v t_1 & t > t_1 \end{cases} \quad (A13)$$

Viscous Shear Stress

$$\tau = C_f q \quad (A14)$$

Limiting Shear Stress

$$\tau^* = \sigma c D g \cos \beta \tan \alpha - \sigma c D g \sin \beta + A_{coh} D^{-3} + \tau_{coh} \quad (A15)$$

Momentum Factor

$$a^{-1} = .5 + \sqrt{.25 + \zeta^{-1}} \quad (A16)$$

$$\zeta = \frac{18\mu_c h}{\sqrt{2} \sigma D^2} \sqrt{\frac{2}{(k+4)RT_c}} \left[1 + \frac{\sqrt{2}}{72e} \frac{C_D(k+4)}{2\pi h^2} \frac{DF}{\mu_c \sqrt{RT_c}} \right] \quad (A17)$$

$$F = \pi r_e^2 p_r \text{ (used only in Equation (A17))} \quad (A18)$$

Viscous Friction Coefficient

$$C_f = a_0 + a_1 \left(\frac{y_{max} - y}{r_e} \right) \left(\frac{y_{max} - y}{y_{max}} \right) \left[\frac{\frac{r}{R_1}}{1 + \left(\frac{r}{R_1} \right)^2} \right] \quad (A19)$$

$$R_1 = (h_1 + a_3 y_{max}) \sqrt{\frac{2}{2+k}} \quad (A20)$$

3. Modifications of Roberts' Theory

In Roberts' formulation of soil erosion, it is assumed the erosion depth y is small compared to the nozzle height h . Thus, no attempt is made to change the flow field as the crater develops. In most applications of this theory, the above assumption is valid. However, during soil erosion experiments the assumption is often violated, and the erosion depth may be even larger than the original nozzle height above the uneroded surface.

In Reference 3, a comparison was made of Roberts' theory with experimental measurements of erosion obtained in a vacuum environment. In some of these tests, the depth of the erosion crater was larger than the hover nozzle height. It was appropriate, therefore, to modify Roberts' formulation to account for the effective increase in nozzle height and changes in the gas flow field. Modifications were selected on physical reasoning and then empirically adjusted by comparison of theoretical predictions and experimental findings. The motivation for the proposed modifications was made as a result of the following observations.

It seemed evident that as the soil eroded and a cavity began forming, the flow field must be altered; and hence, the shear forces acting on the soil also must change. For example, consider the region in the vicinity of the crater lip. One would expect the soil particles on the crater lip to be subjected to larger erosion forces than before the crater was formed. This seems plausible because particles on the crater lip should be exposed to a larger portion of the gas flow than when they were shielded by other particles along the flat surface. Also, such particles are more likely to be impacted by other particles dislodged from the crater itself. These effects should increase the shear forces locally and cause the crater diameter to increase with time, as one observes in erosion experiments and Roberts' theory did not predict. This increased shear force is probably due to both a change in flow and associated dynamic pressure as well as a change in viscous friction coefficient C_f . It was proposed that the changing flow field could be accounted for by simply modifying the friction coefficient. Such a modification is contained in the coefficients a_1 and a_3 in Equations (A19) and (A20). Setting these two coefficients equal to zero reduces these equations to Roberts' formulation. This modification tends to increase the friction coefficient in the vicinity of the crater lip.

Because of the weighting factor r/R_1 , the increase is larger for the outer crater lip than for the inner crater lip. It was found that the values $a_1 = 11$ and $a_3 = .5$ caused the outer crater lip radius to increase with time at a rate similar to that observed during the erosion experiments. The nozzle height h (Equation (A12)) was also modified to allow for an effective increase in nozzle height because of the development of the erosion crater. The empirically determined value for a_2 was about .25. Setting a_2 equal to zero reduces the nozzle height equation to that given by Roberts.

It is obvious that when erosion is small, the preceding modifications become negligible. In the soil erosion calculations performed in this study, the erosion was so small that the modifications were completely negligible.

Another modification is incorporated in the above set of equations through the parameter n in surface pressure Equations (A6) and (A9). Roberts' formulation corresponds to n equal to 1. The parameter n is introduced in an attempt to account for the focusing of the jet when it expands into an atmosphere. When n is larger than unity, both the stagnation pressure p_s and the rate of decay of the pressure along the surface are increased. However, for any value of n , the integrated pressure force on the entire surface is the same.

4. FORTRAN IV Soil Erosion Program

The soil erosion program is called EROS and is written in FORTRAN IV, version 12. It is written to run on an IBM 7094 32K core machine. The program consists of a main program EROS, and five subroutines: AUXSUB, DERIV, SMOOTH, RKAN, and OUTPUT. Below is a brief description of each program.

EROS reads the Input by Namelist name "DATA." EROS saves the first three Runge Kutta integration results. When a successful Adams Moulton integration has been completed, EROS will output those time stations and radial stations specified by the user. After each integration, EROS re-evaluates the upper and lower error bounds (EV and EL) used by RKAM.

AUXSUB calculates the derivative at each radial station. This derivative is then integrated by RKAM to give the depth of the crater (ERODEP) at each radial station.

DERIV calculates the derivative at each radial station of ERODEP vs. RAD (depth vs. radius); the derivative is BETA.

SMOOTH smoothes the beta curve. The curve is smoothed NUMSMT times; if NUMSMT is not input, it is set to 2. (This feature was incorporated because it was found that small irregularities in the erosion crater tended to grow with time as a result of the differentiations to obtain the slope $\beta = \partial y / \partial r$. If uncorrected, these irregularities could lead to numerical instabilities.)

RKAM is a standard TRW subroutine which performs Runge Kutta and Adams Moulton integration. It is used to integrate ERORAT to get ERODEP.

OUTPUT. Since the output from the program can be voluminous, the user may input two quantities, DELMAX and NORAD, to control printed output. The program will write output only at time points which are a multiple of DELMAX. At each output time, every NORADth radial station will be written starting with radial station number one. The output subroutine is used to extrapolate the data, calculated for the present time, to the time point required for output. OUTPUT is called by AUXSUB only if the next time point (TIM+TIMDEL) will lie beyond the next output time. Note that the extrapolated values are used only for OUTPUT and not for calculation.

INPUT

The input is by Namelist name DATA. The following parameters must be input.

<u>FORTRAN</u>	<u>SYMBOL</u>	<u>DEFINITION</u>
GAME	γ	Gas specific heat ratio
AMACH	M_e	Mach number at exit
GASCON	R	Gas constant ($\text{ft}^2/\text{sec}^2 \text{ } {}^\circ\text{R}$)
RADEX	r_e	Exit radius (ft)
GASTEM	T_c	Chamber gas temperature (${}^\circ\text{R}$)
GASVIS	μ_c	Chamber gas viscosity ($\text{lb-sec}/\text{ft}^2$)
PINF	p_o	Ambient pressure (lb/ft^2)
AN	n	Focusing parameter (=1 for lunar environment)
PARSIZ	D	Soil particle size (ft)
DRAGCO	C_D	Particle drag coefficient
SODEN	σ	Soil mass density (slugs/ft^3)
COHSTR	τ_{coh}	Soil cohesive stress (lb/ft^2)
COHPAR	A_{coh}	Cohesion parameter (lb ft)
ALPHA	α	Soil internal friction angle (radians)
A0	a_0	Coefficients in friction coefficient equation
A1	a_1	
SOPAC	c	Soil packing constant (=1 minus porosity)
GRAV	g	Acceleration of gravity (ft/sec^2)
PRES	P_c	Chamber pressure (psf)
HO	h_0	Initial height of nozzle (ft)
HHOVER	h_1	Hover (engine cutoff) height (ft)
HVTIM	t_1	Time at which hover/cutoff begins (sec)
FINTIM	T	Final time (sec)
VEL	V_V	Descent velocity (ft/sec)
A2	a_2	Input non-dimensional parameter in R_1 (equation)
A3	a_3	Input non-dimensional parameter in $h(t)$ (equation)
EPS	ϵ	Distance to first radial station (must be greater than zero because of the singularity at $r = 0$, ft)

<u>FORTRAN</u>	<u>SYMBOL</u>	<u>DEFINITION</u>
NUMRAD		Number of radial stations
NUMSMT		Number of times beta curve is smooth
DELMIN		Minimum time increment (sec)
DELMAX		Maximum time increment also step size for controlling output (sec)
RADIUS		Radius to last radial station (ft)
DELTIM		Initial time increment ($DELMIN \leq DELTIM \leq DELMAX$)
NORAD		Increment for writing out selective radial stations. (Integer). 1st radial station and every NORADth station thereafter is written
ERRUP		Reciprocal of % of depth for upper error bound
ERRLO		Reciprocal of % of depth for lower error bound, $DELMIN \leq DELMAX$

OPERATING PROCEDURE

The program will accept stacked cases.

The following parameters must be considered when evaluating running time for the program: ERRUP, ERRLO, DELMIN, DELMAX, NORAD, and FINTIM. Unfortunately the first four also control the accuracy of the results.

The looser the error bounds, the faster the program runs. On test cases, $\text{ERRUP} \leq 25$ changed the results significantly.

A reasonable upper bound on the run time is 120 times FINTIM where FINTIM is in seconds.

Concerning errors, it seems best on the first run to set $\text{ERRUP} = 50$; and if the results seem unreasonable, increase ERRUP .

To have reasonable error control, the following inequalities should hold:

$$\text{ERRUP} \leq 50$$

$$\text{ERRLO} \geq 32 \text{ ERRUP}$$

Note that ERRUP is used to compute the upper bound of allowable error at each integration. It is not an upper bound for the cumulative error.

The program listing follows:

EROS

11/11/67

EXTERNAL AUXSUB	00000010
DIMENSION TEMP(150),TEMP1(150)	00000030
DOUBLE PRECISION TIM,TIMDEL,HOLD	00000040
COMMON/OUTPUT/DEPTH(150,3),RATE(150,3),TIME(3),UU(150,3),	00000050
1SURF(150,3),DYNAM(150,3),RH00(150,3),HEIGHT(3),AAA(3),	00000060
2STAG(3),PTOT(150,3),	00000070
3TFMPS(9,150),EU(150),EL(150),AUU(150,3),BETAA(150,3)	00000080
COMMON/PARAM/THET(150),BETA(150),PRESUR(150),	00000090
1DYPRES(150),U(150),RHO(150),FRICCO(150),TAU(150),TAUSTR(150),	00000100
2ERORAT(150),RAD(150),ERODEP(150),AA,GAMA,AMACH,GASCON,GAM1,	00000110
3RADCY,GASTEM,GASVIS,PINF,AN,PARSIZ,DRAGCO,SODEN,	00000120
4COHSTR,COHPAR,ALPHA,AC,A1,SOPAC,GRAV,PRES,HO,HHOVER,	00000130
5HVTIM,FINTIM,VEL,A2,A3,EPS,NUMRAD,NUMSMT,REPRES,	00000140
6ENGPAR,F,YMAX,L,STAGPR,H,TIM,H1 NAMELIST/DATA/GAMA,AMACH,GASCON,RADEX,GASTEM,GASVIS,	00000150
1PINF,AN,PARSIZ,DRAGCO,SODEN,COHSTR,CCHPAR,ALPHA,AD,	00000160
2A1,SOPAC,GRAV,PRES,HO,HHOVER,HVTIM,FINTIM,VEL,A2,	00000170
3A3,FPS,NUMRAD,NUMSMT,DELMIN,DELMAX,RAIUS,DELTIM,NURAD,	00000180
4FRRUP,FRRLO DATA PI/3.14159267	00000190
DATA FRRUP,FRRLO/100.,200./	00000200
1 READ (2,DATA)	00000210
C***** INITIALIZE ARRAYS	00000220
TIMDEL=DELTIM	00000230 1
IF (TIMDEL.LE.0.) GO TO 400	00000240 2
A=NUMRAD	00000250 3
IF (NORAD.LT.1) NORAD=1	00000260 6
IF (NUMSMT.LT.1) NUMSMT=2	00000270 7
DO 5 I=1,NUMRAD	00000280 10
ERORAT(I)=C.	00000290 13
ERODEP(I)=C.	00000300 14
TEMPS(1,I)=0.	00000310 15
FU(I)=.05	00000320 16
FL(I)=.05	00000330 17
R1=I-1	00000340 18
RAD(I)=R1*RADIUS/A	00000350 19
	00000360 20

EROS

11/11/67

5	CONTINUE	00000370	21
	GAM1=(GAMA-1.)/GAMA	00000380	23
	B2=AMACH*AMACH	00000390	24
	B1=(1.+GAMA-1.)/2.*B2)**(1./GAM1)	00000400	25
	REPRES=(1.+GAMA*B2)*PRES/B1	00000410	26
	ENGPAR=GAMA*(GAMA-1.)*B2	00000420	27
	F=PI*RADEX*RADEX*REPRES	00000430	28
	RAD(1)=EPS	00000440	29
	IFLG=-1	00000450	30
	IFLG2=0		31
	TIM=0.	00000460	32
	YMAX=0.	00000470	33
	HOLDI=DELMAX	00000480	34
10	ICNT=0	00000500	35
11	CALL RKAM (TIM,TIMDEL,ERODEP,ERORAT,AUXSUB, INUMRAD,0.EU,EL,DELMAX,DELMIN,ICNT,TEMPS,NH) IF (ICNT.LF.3.AND.IFLG.NE.1) GO TO 15 IF (IFLG.EQ.-1) IFLG=0 GO TO 200	00000510 00000520 00000530 00000540 00000550	36 37 40 41 42
	C***** SAVE FIRST THREE RUNGE KUTTA RESULTS	00000560	
	C***** UNTIL WE HAVE A SUCCESSFUL ADAMS MOULTON RESULT	00000570	43
15	L=ICNT	00000580	44
	TIME(L)=TIM	00000590	45
	HFIGHT(L)=H1	00000600	46
	AAA(L)=AA	00000610	47
	STAG(L)=STAGPR/144.		48
	DO 20 I=1,NUMRAD	00000630	49
	DFPTH(I,L)=ERODEP(I)	00000640	50
	RATE(I,L)=ERORAT(I)	00000650	51
	UU(I,L)=U(I)	00000660	52
	RHO0(I,L)=RHO(I)	00000670	53
	AU(I,I)=AA*U(I)	00000680	54
	BFTAA(I,L)=BETA(I)*57.29577	00000690	55
	DYNAM(I,L)=DYPRES(I)/144.	00000700	56
	SURF(I,L)=PRESUR(I)*STAGPR/144.	00000710	57
	PTOT(I,L)= SURF(I,L)+PINF /144.	00000720	58
20	CONTINUF	00000730	59

EROS

11/11/67

200	IF (IFLG)305,240,250	00000740
***** WRITE ALL THE SAVED VALUES		00000750
240	B1=REPRFS/144.	61
	WRITE (3,700) ENGPAR,B1	00000760
	DO 245 L=1,3	62
	IFLG1=0	00000770
	IF (L,F0,1,OR,TIME(L),EQ,HOLD1) GO TO 242	63
	IF (TIME(L)+TIMDEL,LE,HOLD1) GO TO 245	00000780
	DO 230 I=1,NUMRAD	66
	TEMP1(I)=FR0RAT(I)	67
230	TEMP(I)=ER0DFP(I)	00000800
	IFLG1=1	68
	CALL OUT (DEPTH(I,L),L,HOLD1,1,TIMDEL,TEMP1)	71
242	IF (HEIGHT(L),GT,HHOVER) WRITE (3,701)	00000830
	IF (L,NE,1) HOLD1=HOLD1+DELMAX	74
243	IF (HEIGHT(L),LE,HHOVER) WRITE (3,702)	75
	WRITE (3,703) HEIGHT(L),TIME(L),AAA(L),STAG(L)	00000840
	WRITE (3,704)	76
	DO 244 I=1,NUMRAD,NORAD	78
244	WRITE (3,705) RAD(I),DEPTH(I,L),BETAA(I,L),RATE(I,L),	79
	1SURF(I,L),DYNAM(I,L),RHOO(I,L),AUU(I,L),UU(I,L),PTOT(I,L)	00000860
	IF (IFLG1,EQ,0) GO TO 245	80
	DO 235 I=1,NUMRAD	00000870
	ER0RAT(I)=TEMP1(I)	84
235	FR0DEP(I)=TEMP(I)	00000880
245	CONTINUE	91
	IFLG=1	00000900
***** WRITE CURRENT VALUE		94
250	CONTINUE	00000910
	IFLG1=0	96
	TTIM=TIM	00000920
	IF (TIM,F0,HOLD1) GO TO 252	97
	IF (IFLG2,EQ,1) GO TO 221	101
	IF (TIM+TIMDEL,LE,H0VTIM) GO TO 221	104
	IFLG2=1	105
	HOLD2=H0VTIM	106
	DO 215 I=1,NUMRAD	108
		00000970
		00000980
		00000990
		00001000
		00001020
		00001040
		110
		111
		112
		113
		114
		117
		120
		123
		124
		125

A
-15

EROS

11/11/67

	TEMP1(I)=ERORAT(I)	126
215	TEMP(I)=ERODEP(I)	127
	IFLG1=1	129
	CALL OUT (ERODEP.L.HOLD2.2.TIMDEL TEMP1)	130
	WRITE (3.702)	131
	TTIM=HOVTIM	133
	IF (HOVTIM.EQ.HOLD1) HOLD1=HOLD1+DELMAX	134
	GO TO 216	137
221	IF (TIM+TIMDEL.LE.HOLD1) GO TO 255	138
	DO 220 I=1.NUMRAD	00001060 141
	TEMP1(I)=ERORAT(I)	142
220	TEMP(I)=ERODEP(I)	00001070 143
	IFLG1=1	00001080 145
	CALL OUT (ERODEP.L.HOLD1.2.TIMDEL TEMP1)	146
252	IF (HOLD1.LT.HOVTIM) WRITE (3.701)	147
	TTIM=HOLD1	00001110 151
253	IF (HOLD1.GE.HOVTIM) WRITE (3.702)	152
	HOLD1=HOLD1+DELMAX	00001120 156
216	CONTINUE	157
	B3=STAGPR/144.	158
	WRITE (3.703) HI.TTIM.AA.B3	159
	WRITE (3.704)	00001150 162
	DO 254 I=1.NUMRAD.NORAD	00001160 164
	B1=BETA(I)*57.29577	00001170 165
	B2=AA*U(I)	00001180 166
	B3=PRESUR(I)*STAGPR/144.	00001190 167
	B4=B3+PINF/144.	00001200 168
	B5=DYPRES(I)/144.	00001210 169
	WRITE (3.705) RAD(I).ERODEP(I).B1.ERORAT(I).B3. B5.	00001220
	IRHO(I).B2.U(I).B4	00001230 170
254	CONTINUE	00001240 173
	IF (IFLG1.EQ.0) GO TO 255	00001250 175
	DO 225 I=1.NUMRAD	00001260 178
	ERORAT(I)=TEMP1(I)	179
225	ERODEP(I)=TEMP(I)	00001270 180
255	CONTINUE	00001280
	C***** SET NEW ERROR BOUNDS FOR RKAM	00001290 182

A-17
EROS

11/11/67

305 YMAX=FRDDEP(1) 00001300 183
DO 310 I=1,NUMRAD 00001310 184
EU(I)=ABS(ERODEP(I)/ERRUP) 00001320 185
FL(I)=ABS(ERODEP(I)/ERRLO) 00001330 186
YMAX=AMAX1(YMAX,ERODEP(I)) 00001340 187
310 CONTINUE 00001350
C***** IF NECESSARY ADJUST TIME INCREMENT ON 00001360
C***** LAST PASS 00001370 188
IF (TIM.GE.FINTIM) GO TO 1 00001380 190
IF (FINTIM-TIM-TIMDEL)320,11,11 00001390 193
320 TIMDEL=FINTIM-TIM 00001400 194
GO TO 10 00001410 195
400 WRITF (3.706) 00001420 196
GO TO 1 00001430 198
700 FORMAT (35H1 ENGINE PARAMETER =E15.8//
135H ' RECOVERY PRESSURE (PSI) =E15.8///.
701 FORMAT (//15H DESCENDING//) 00001450
702 FORMAT (//13H HOVERING//) 00001460
703 FORMAT (30H NOZZLE HEIGHT (FT) =E15.8,21X,
16HTIME =F10.4//30H MOMENTUM FACTOR A =E15.8, 00001470
210X.27HSTAGNATION PRESSURE (PSI) =E15.8) 00001480
704 FORMAT (///51X.5HSURF..8X,4HDYN..20X,5HPART.,7X,3HGAS,9X,5HTOTAL/
1 12H STATION 12H DEPTH 12H SLOPE 12H RATE 00001490
2 12H PRESS. 12H PRESS. 12H GAS DENS. 12H VEL. 00001500
3 12H VFL. 12H PRESS. /12H (FT) 12H (FT) 00001510
4 12H (DEG) 12H (FT/SEC) 12H (PSI) 12H (PSI) 00001520
5 12H SLUG/CU FT 12H (FT/SEC) 12H (FT/SEC) 12H (PSI) //) 00001530
705 FORMAT (10(1X,E11.4)) 00001540
706 FORMAT (61H NO TIME INCREMENT (DELTIM) FOR CASE. I'M GOING TO NEX00001580
1T CASF) 00001550
END 00001560
00001570
00001580
00001590
00001600 199

AUXSUB

10/26/67

SUBROUTINE AUXSJR (ICNT)	00000010
DOUBLE PRECISION TIM,TIMDEL	00000020
COMMON/PARAM/THET(150),BETA(150),PRESUR(150),	00000030
1DYPRES(150),U(150),RHO(150),FRICCO(150),TAU(150),TAUSTR(150),	00000040
2ERORAT(150),RAD(150),ERODEP(150),AA,GAMA,AMASH,GASCON,GAMI,	00000050
3RADEX,GASTEM,GASVIS,PINF,AN,PARSIZ,DRAGCO,SDDEN,	00000060
4COHSTR,COHPAR,ALPHA,AC,A1,SOPAC,GRAV,PRES,H0,HHOVER,	00000070
5HOVTIM,FINTIM,VEL,A2,A3,EPS,NUMRAD,NUMSMT,REPRES,	00000080
6ENGPART,F,YMAX,L,STAGPR,H,TIM,H1	00000090
DATA PI/3.1415926/	00000100
IF (ICNT.NE.1) GO TO 5	00000110
IF (L.NE.1) YMAX=0.	00000120
5 CONTINUE	00000130
C***** CALCULATE PARAMETERS THAT ARE CONSTANT WITH	00000140
C***** RESPECT TO RADIUS	00000150
IF (TIM-HOVTIM) 1,1,2	00000160
1 H1=HC-VEL*TIM	00000170
GO TO 3	00000180
2 H1=HC-VEL*HOVTIM	00000190
3 H=H1+A2*YMAX	00000200
R1=(H1+A3*YMAX)*SQRT(2./(2.+ENGPART))	00000210
B1=(AN*(ENGPART+4.)-2.)/2.*REPRES*((RADEX+1)**2)	00000220
STAGPR=AMIN1(REPRES,B1)	00000230
B1=18.*GASVIS*H/(1.414214*SDDEN*PARSIZ*PARSIZ)	00000240
B2=SQRT(2./((ENGPART+4.)*GASCON*GASTEM))	00000250
B3=1.+1.414214/195.7162*DRAGCO*(ENGPART+4.)/	00000260
1 (2.*PI*H*H)*PARSIZ*F/(GASVIS*SQRT(GASCON*GASTEM))	00000270
ZETA=B1*B2*B3	00000280
AA=1./(.5+SQRT(.25+1./ZETA))	00000290
C***** CALCULATE PARAMETERS AT RADIAL STATIONS	00000300
DO 20 I=1,NUMRAD	00000310
20 THET(I)=ATAN2(RAD(I),H)	00000320
C***** BETA IS SLOPE OF ERODEP VS. RAD	00000330
CALL DERIV (ERODEP,RAD,BETA,NUMRAD)	00000340
DO 30 I=1,NUMRAD	00000350
30 BETA(I)=ATAN(BETA(I))	00000360

AUXSUB

10/26/67

C***** SMOOTH BETA CURVE NUMSMT = NUMBER OF TIMES
C***** CURVE IS SMOOTHED
CALL SMOOTH (BETA,NUMRAD,NUMSMT)
C***** CALCULATE THE DERIVATIVE AT EACH RADIAL STATION
DO 40 I=1,NUMRAD
B1=COS(THET(I))**(AN*(ENGPAR+4.))*(COS(BETA(I))**2)
PRESUR(I)=B1*((1.-TAN(THET(I))*TAN(BETA(I)))**2)
DYPRES(I)=1./GAM1*(1.-(PRESUR(I)**GAM1))*STASPR*
I (PRESUR(I)**(1./GAMA))
B1=(2./GAM1)*GASCJN*GASTEM*(1.-PRESUR(I)**GA41)
U(I)=B1**.5
RHO(I)=2.*DYPRES(I)/(U(I)*U(I))
B1=RAD(I)/R1
FRICCO(I)=A0+A1*((YMAX-ERODEP(I))**2)/
I (RADEX*YMAX)*B1/(1.+B1*B1)
IF (YMAX.LE.C.) FRICCO(I)=A0
TAU(I)=FRICCO(I)*DYPRES(I)
B1=SODEN*PARSIZ *SOPAC*GRAV
B2=COS(BETA(I))*TAN(ALPHA)-SIN(BETA(I))
TAUSTR(I)=B1*B2+COHPAR/(PARSIZ**3)+COHSTR
IF (TAU(I)-TAUSTR(I)) 34,34,35
34 ERORAT(I)=C.
GO TO 40
35 ERORAT(I)=2.*(TAU(I)-TAUSTR(I))/(AA*SODEN*
I SOPAC*U(I)*COS(BETA(I)))
40 CONTINUE
RETURN
END

00000370
00000380 26
00000390
00000400 28
00000410 29
00000420 30
00000430 31
00000440
00000450 32
00000460 33
00000470 34
00000480 35
00000490 36
00000500
00000510 37
00000520 38
00000530 41
00000540 42
00000550 43
00000560 44
00000570 45
00000580 46
00000590
00000600 48
00000610 49
00000620 51
00000630 52

DERIV

10/09/67

SUBROUTINE DERIV (Y,RAD,BETA,N)

C***** BETA IS SLOPE OF Y VS. RAD

DIMENSION Y(N),RAD(N),BETA(N)

C***** N MUST BE GREATER THAN OR EQUAL TO 5

IF (N.LT.5) GO TO 100

H=12.*(RAD(2)-RAD(1))

BETA(1)=(-25.*Y(1)+48.*Y(2)-36.*Y(3)+16.*Y(4)-3.*Y(5))/H

H=12.*(RAD(3)-RAD(2))

BETA(2)=(-3.*Y(1)-10.*Y(2)+18.*Y(3)-6.*Y(4)+Y(5))/H

NNK=N-2

DO 1 I=3,NNK

BETA(I)=(Y(I-2)-8.*Y(I-1)+8.*Y(I+1)-Y(I+2))/H

BETA(N-1)=(-Y(N-4)+6.*Y(N-3)-18.*Y(N-2)+10.*Y(N-1)+3.*Y(N))/H

BETA(N)=(3.*Y(N-4)-16.*Y(N-3)+36.*Y(N-2)-48.*Y(N-1)

+25.*Y(N))/H

RETURN

100 WRITE (3,101)

101 FCRMAT (37H IN SUBROUTINE DERIV N IS LESS THAN 5)

RETURN

END

1
4
5
6
7
8
9
10
12
13
14
15
17
18

SMOOTH

10/24/67

SUBROUTINE SMOOTH (BETA,N,NN)
DIMENSTION BETA(N),S(150)
IF (N.LT.5) GO TO 100
DO 2 JJ=1,NN
1 R(1)=(69.*BETA(1)+4.*BETA(2)-6.*BETA(3)+4.*BETA(4)-BETA(5))
1 /70.
1 R(2)=(2.*BETA(1)+27.*BETA(2)+12.*BETA(3)-8.*BETA(4)+2.
1 *BETA(5))/35.
1 NNK=N-2
1 DO 1 I=3,NNK
1 R(I)=(-3.*BETA(I-2)+12.*BETA(I-1)+17.*BETA(I)+
1 12.*BETA(I+1)-3.*BETA(I+2))/35.
1 R(N-1)=(2.*BETA(N)+27.*BETA(N-1)+12.*BETA(N-2)
1 -8.*BETA(N-3)+2.*BETA(N-4))/35.
1 R(N)=(69.*BETA(N)+4.*BETA(N-1)-6.*BETA(N-2)
1 +4.*BETA(N-3)-BETA(N-4))/70.
1 DO 3 I=1,N
3 BETA(I)=R(I)
2 CONTINUE
RETURN
100 WRITE (3,101)
101 FFORMAT (3RH TN SUBROUTINE SMOOTH N IS LESS THAN 5)
RETURN
END

A-21

RKAM

10/04/67

SUBROUTINE RKAM(XDP,HDP,VAR,DER,AUXSUB,N,OPT,
!FU,EL,HMAX,HMIN,ICNT,TEMPS,NH)
DOUBLE PRECISION XDP,HDP,CDP
DIMENSION VAR(1),DEP(1),FU(1),EL(1),TEMPS(9,1),C(?)
FOUTVALENCE(CDP,C)
NN=N
C EXIT IF N IS ZERO OR NEGATIVE
IF(NN.LT.0) RETURN
IC=ICNT
C TRANSFER ON R-K ONLY OPTION
IF(OPT.NE.0.0) GO TO 200
IF(IC.GT.2) GO TO 110
C COUNTER IS LESS THAN 2--RUNGA-KUTTA STEP
K=1
IC=IC+1
IF(IC.GT.1) GO TO 120
C COUNTER WAS ZERO ON ENTRY--STORE INITIAL ORDINATES
100 DO 105 I=1,NN
TEMPS(5,I)=TEMPS(1,I)
105 TEMPS(6,I)=VAR(I)
GO TO 120
C COUNTER IS GREATER THAN 2--ADAMS-MOULTON STEP
C STORE ENTRY ORDINATES
110 DO 115 I=1,NN
TEMPS(2,I)=VAR(I)
115 TEMPS(3,I)=TEMPS(1,I)
K=0
C STORE ENTRY DERIVATIVES
120 DO 125 I=1,NN
125 TEMPS(4,I)=DFR(I)
IF(K.EQ.0) GO TO 300
C INTEGRATE ONE STEP WITH P-K
200 K=C
DO 205 I=1,NN
TEMPS(2,I)=VAR(I)
205 TEMPS(3,I)=DFR(I)

RKAM0002	
RKAM0003	
RKAM0004	
RKAM0005	
RKAM0006	
RKAM0007	
RKAM0008	1
RKAM0009	2
RKAM0010	
RKAM0011	5
RKAM0012	6
RKAM0013	
RKAM0014	9
RKAM0015	12
RKAM0016	13
RKAM0017	
RKAM0018	14
RKAM0019	17
RKAM0020	18
RKAM0021	19
RKAM0022	
RKAM0023	21
RKAM0024	22
RKAM0025	23
RKAM0026	24
RKAM0027	
RKAM0028	26
RKAM0029	
RKAM0030	27
RKAM0031	28
RKAM0032	
RKAM0033	30
RKAM0034	33
RKAM0035	34
RKAM0036	35
RKAM0037	36

PKAM

```

CDD=HDP/2.00
A=C(1)
210 XDP=XDP+CDD
215 DO 220 T=1,NN
220 VAR(I)=TEMPS(2,I)+A*DER(I)
CALL AUXSUB (IC)
K=K+1
IF(K.EQ.3) GO TO 230
DO 225 T=1,NN
225 TEMPS(3,I)=TEMPS(3,I)+2.0*DER(I)
IF(K.EQ.1) GO TO 215
A=HDP
GO TO 210
230 A=A/6.0
DO 235 I=1,NN
C(1)=TEMPS(2,I)
C(2)=TEMPS(1,I)
R=(TEMPS(3,I)+DER(I))*A
CDD=CDD+R
VAR(I)=C(1)
235 TEMPS(1,I)=C(2)
CALL AUXSUB (IC)
IF(NOPT.NE.0.0) RETURN
GO TO 600
C INTEGRATE ONE STEP WITH A=M AND TEST STEP SIZE
300 A=HDP/24.0
XDP=XDP+HDP
DO 310 T=1,NN
TEMPS(1,I)=A*(55.0*TEMPS(4,I)-59.0*TEMPS(5,I)
  +37.0*TEMPS(6,I)-9.0*TEMPS(7,I))
C(1)=TEMPS(2,I)
C(2)=TEMPS(3,I)
310 VAR(I)=CDD+TEMPS(1,I)
CALL AUXSUB (IC)
K=0
DO 325 T=1,NN
R=A*(9.0*DER(I)+10.0*TEMPS(4,I)-5.0*TEMPS(5,I)+TEMPS(6,I))

```

10/04/67

RKAM0038	38
RKAM0039	39
RKAM0040	40
RKAM0041	41
RKAM0042	42
	44
RKAM0044	45
RKAM0045	46
RKAM0046	49
RKAM0047	50
RKAM0048	52
RKAM0049	55
RKAM0050	56
RKAM0051	57
RKAM0052	58
RKAM0053	59
RKAM0054	60
RKAM0055	61
RKAM0056	62
RKAM0057	63
RKAM0058	64
	66
RKAM0060	67
RKAM0061	
RKAM0062	70
RKAM0063	71
RKAM0064	72
RKAM0065	73
RKAM0066	
RKAM0067	74
RKAM0068	75
RKAM0069	76
RKAM0070	77
	79
RKAM0072	80
RKAM0073	81
RKAM0074	82

A-24

RKAM

```

C=ABS(R-TEMPS(1,I))
IF(C.LT.EU(I)) GO TO 320
K=1
IF(C.LT.EU(I)) GO TO 320
IF(ABS(HDP).GT.(2.*HMIN)) GO TO 500
320 C(1)=TEMPS(2,I)
C(2)=TEMPS(3,I)
CDP=CDP+R
VAR(I)=C(1)
325 TEMPS(1,I)=C(2)
CALL AIIXSUB (IC)
IF(IC.GT.3) GO TO 330
IC=4
330 IF(K.EQ.0) GO TO 340
IC=4
GO TO 600
340 IC=IC+1
IF(IC.LT.7) GO TO 600
IF(ABS(HDP).GT.(HMAX/2.0)) GO TO 600
C DOUBLING PROCESS--REARRANGE DERIVATIVES AND EXIT
400 IC=4
HDP=HDP*2.000
DO 410 I=1,NN
TEMPS(6,I)=TEMPS(7,I)
410 TEMPS(7,I)=TEMPS(9,I)
GO TO 700
C HALVING PROCESS
C COUNTER L.T. 4--PACK 3 STEPS--RESTART R-K WITH H/2
C COUNTER G.T. 3--INTERPOLATE--REDO LAST STEP WITH H/2
500 CDP=HDP
NH=1
HDP=HDP/2.000
IF(IC.GE.4) GO TO 520
IC=1
XDP=XDP-4.000*CDP
DO 510 I=1,NN
VAR(I)=TEMPS(9,I)

```

10/24/67

RKAM0075	83
RKAM0076	84
RKAM0077	87
RKAM0078	88
RKAM0079	91
RKAM0080	94
RKAM0081	95
RKAM0082	96
RKAM0083	97
RKAM0084	98
	100
RKAM0086	101
RKAM0087	104
RKAM0088	105
RKAM0089	108
RKAM0090	109
RKAM0091	110
RKAM0092	111
RKAM0093	
RKAM0094	114
RKAM0095	117
RKAM0096	118
RKAM0097	119
RKAM0098	120
RKAM0099	121
RKAM0100	
RKAM0101	
RKAM0102	
RKAM0103	123
RKAM0104	124
RKAM0105	125
RKAM0106	126
RKAM0107	127
RKAM0108	130
RKAM0109	131
RKAM0110	132
RKAM0111	133

OKAM

510 TEMPS(1,T)=TEMPS(8,T)
510 DER(T)=TEMPS(7,T)
GO TO 100
520 XDP=XDP-CDD
TC=4
DO F20 I=1,NN
A=(5.*TEMPS(4,T)+2.*TEMPS(5,T)-TEMPS(6,T)+TEMPS(7,T))/15.0
TEMPS(7,T)=(9.*TEMPS(5,T)+TEMPS(6,T))-TEMPS(4,T)-TEMPS(7,T)/15.0
TEMPS(6,T)=TEMPS(5,T)
530 TEMPS(5,T)=A
GO TO 300
C MOVE PAST DATA
600 DO 610 J=1,5
K=10-J
DO 610 T=1,NN
610 TEMPS(K,T)=TEMPS(K-1,T)
700 ICNT=IC
705 RETURN
END

A-25

10/04/67

RKAM0112 134
RKAM0113 135
RKAM0114 137
RKAM0115 138
RKAM0116 139
RKAM0117 140
RKAM0118 141
RKAM0119 142
RKAM0120 143
RKAM0121 144
RKAM0122 145
RKAM0123 146
RKAM0124 147
RKAM0125 148
RKAM0126 149
RKAM0127 150
RKAM0128 153
RKAM0129 154
RKAM0130 155

OUT

11/09/67

```

SUBROUTINE OUT (HOLE,L,HOLD1,NBRAN,TIMDEL,TEMP1)
DIMENSION HOLE(1),B(4),TEMP1(1)
DOUBLE PRECISION TIM,TIMDEL,HOLD1,TTIM
COMMON/OUTPUT/DEPTH(150,3),RATE(150,3),TIME(3),UU(150,3),
1SURF(150,3),DYNAM(150,3),RHOO(150,3),HEIGHT(3),AAA(3),
2STAG(3),PTOT(150,3),
3TEMPS(9,150),EU(150),EL(150),AUU(150,3),BETAA(150,3)
COMMON/PARAM/THET(150),BETA(150),PRESUR(150),
1DYPRES(150),U(150),RHO(150),FRICCO(150),TAU(150),TAUSTR(150),
2ERORAT(150),RAD(150),ERODEP(150),AA,GAMA,AMACH,GASCON,GAM1,
3RADFX,GASTEM,GASVIS,PINF,AN,PARSIZ,DRAGCO,SODEN,
4COHSTR,COHPAR,ALPHA,A0,A1,SOPAC,GRAV,PRES,HO,HHOVER,
5SHOVTIM,FINTIM,VEL,A2,A3,EPS,NUMRAD,NUMSMT,REPRES,
6ENGPAR,F,YMAX,L,STAGPR,H,TIM,HI
      IF (NBRAN.EQ.2) GO TO 10
      DO 5 I=1,NUMRAD
      5 ERODEP(I)=HOLE(I)
      10 CONTINUE
      YYMAX=YMAX
      YMAX=ERODEP(1)
      DO 11 I=1,NUMRAD
      11 YMAX=AMAX1(ERODEP(I),YMAX)
      TTIM=TIM
      TIM=HOLD1
      CALL AUXSUB (5)
      TIM=TTIM
      YMAX=YYMAX
      S=(HOLD1-TIM)/TIMDEL
      B(1)=S*S*S+8.*S*S+22.*S+24.
      B(2)=-S*(3.*S*S+20.*S+36.)
      B(3)=S*(3.*S*S+16.*S+18.)
      B(4)=-S*(S+2.)*(S+2.)
      DO 15 I=1,NUMRAD
      15 SUM=TEMP1(I)
      DO 12 J=2,4
      12 SUM=SUM+B(J)*TEMPS(J+3,I)
      00000030
      00000040
      00000050
      00000060
      00000070
      00000080
      00000090
      00000100
      00000110
      00000120
      00000130
      00000140
      00000150
      00000160
      00000170
      00000180
      00000190
      00000200
      00000210
      00000220
      00000230
      00000240
      00000250
      00000260
      00000270
      00000280
      00000290
      00000300
      00000310
      00000320
      00000330
      00000340
      00000350
      00000360
      1
      4
      5
      7
      8
      9
      10
      11
      13
      14
      15
      16
      17
      18
      19
      20
      21
      22
      23
      24
      25
      26

```

DUT

```
15 ERODEP(I)=ERODEP(I)+SUM*(HOLD1-TIM)/24.  
CONTINUE  
IF (NBRAN.EQ.2) RETURN  
TIME(L)=HOLD1  
HEIGHT(L)=H1  
AAA(L)=AA  
STAG(L)=STAGPR/144.  
DO 20 I=1,NUMRAD  
DEPTH(I,L)=ERODEP(I)  
RATE(I,L)=ERORAT(I)  
UJ(I,L)=U(I)  
RHOO(I,L)=RHO(I)  
AJU(I,L)=AA*U(I)  
BFTAA(I,L)=BETA(I)*57.29577  
DYNAM(I,L)=DYPRES(I)/144.  
SURF(I,L)=PRESUR(I)*STAGPR/144.  
PTOT(I,L)= SURF(I,L)+PINF /144.  
20 CONTINUE  
RETURN  
END
```

11/09/67

00000370	28
00000380	29
00000390	31
00000400	34
00000410	35
00000420	36
	37
00000440	38
00000450	39
00000460	40
00000470	41
00000480	42
00000490	43
00000500	44
00000510	45
00000520	46
00000530	47
00000540	48
00000550	50
00000560	51

5. Example FORTRAN IV Soil Erosion Calculations

Example calculations are presented in this section for the following parameter values

$\gamma = 1.252$	$n = 1$
$M_e = 3.98$	$a_0 = .2$
$R = 2310 \text{ ft}^2/\text{sec}^2 {}^\circ\text{R}$	$a_1 = 0$
$r_e = .389 \text{ ft}$	$a_2 = 0$
$T_c = 5670 {}^\circ\text{R}$	$a_3 = 0$
$\mu_c = 1 \times 10^{-6} \text{ lb-sec/ft}^2$	$c = .5$
$\alpha = 34 \text{ deg } (0.593 \text{ rad})$	$C_D = 2$
$g = 12.3 \text{ ft/sec}^2$	$A_{coh} = 0$
$\sigma = 5.81 \text{ slugs/ft}^3$	$\tau_{coh} = 0$
$h_o = 40 \text{ ft}^*$	$V_v = 5 \text{ ft/sec}$
$p_o = .0726 \text{ psia } (10.45 \text{ psf})$	$p_c = 42.5 \text{ psia } (6120 \text{ psf})$
$D = 300 \text{ microns } (0.000984 \text{ ft})$	

The first output data sheet lists the input parameters, the computed value of k , recovery pressure p_r , and the soil erosion data at $t = 0.1 \text{ sec}$ ($h = 39.5 \text{ ft}$). The second output data sheet shows the erosion data at $t = 2 \text{ sec}$ ($h = 30 \text{ ft}$) and $t = 4 \text{ sec}$ ($h = 20 \text{ ft}$). The output data are the radial station r , erosion depth y , erosion crater slope β , erosion rate y , surface pressure p , dynamic pressure q , gas density ρ , soil particle velocity v , gas velocity u , and total surface pressure $p + p_g$. Also shown are the momentum factor "a" and stagnation pressure p_s at the various nozzle heights.

* An initial nozzle height of 40 feet, rather than 100 feet, was used in this example, because no erosion takes place above a 40-foot nozzle height for the 300 micron particles. Observe, for example, on pages A-29 and A-30 that the erosion rate is zero at all radial stations at the 40-foot nozzle height, while soil is eroding at a 30-foot nozzle height.

SYSTEMS

SDATA
GAMA=1.252, A4ACH=3.58, GASCON=2310., RADEX=.389,
GASTEM=5670., GASVIS=1.E-6, PTINF=10.45, AN=1,
PARSIZ=.000984, DRAGCN=2., SDEN=5.91, COHSTR=0.,
COHPAR=0., ALPHA=.502348, A0=.2, A1=0., A2=0., A3=0.,
SOPAC=.5, GRAV=12.3, PRES=6120., H0=40.,
HHOVER=15., HOVTIM=5., FINTIM=4., VEL=5.,
EPS=1.E-5, NUMRAD=12, NOPAD=1, NUMSMT=2,
RADIUS=24., DELMIN=.1, DELMAX=2., DELTIM=.1,
ERRUP=50., ERRLO=400., \$END

EJECTING PARAMETER = 0.4997292E 01

RECOVERY PRESSURE (PSI) = 0.37585849E 01

DESCENDING

NOZZLE HEIGHT (FT) = 0.39501000E 02

TIME = 0.1000

MOMENTUM FACTOR A = 0.10228068E-00

STAGNATION PRESSURE (PSI) = 0.12889994E-02

STATION (FT)	DEPTH (FT)	SLOPE (DEG)	RATE (FT/SEC)	SURF. PRESS. (PSI)	DYN. PRESS. (PSI)	GAS DENS. SLUG/CU FT	PART. VEL. (FT/SEC)	GAS VEL. (FT/SEC)	TOTAL PRESS. (PSI)
0.1000E-04	0.	-0.	0.	0.1299E-02	-0.	-0.	-0.	-0.	0.7386E-01
0.2000E 01	0.	-0.	0.	0.1274E-02	0.1469E-04	0.1404E-07	0.5615E 02	0.5490E 03	0.7384E-01
0.4000E 01	0.	-0.	0.	0.1231E-02	0.5577E-04	0.1366E-07	0.1119E 03	0.1094E 04	0.7380E-01
0.5000E 01	0.	-0.	0.	0.1163E-02	0.1206E-03	0.1306E-07	0.1668E 03	0.1631E 04	0.7373E-01
0.8000E 01	0.	-0.	0.	0.1076E-02	0.1981E-03	0.1227E-07	0.2206E 03	0.2157E 04	0.7365E-01
0.1000E 02	0.	-0.	0.	0.9747E-03	0.2802E-03	0.1134E-07	0.2729E 03	0.2668E 04	0.7354E-01
0.1200E 02	0.	-0.	0.	0.9665E-03	0.3583E-03	0.1032E-07	0.3234E 03	0.3162E 04	0.7344E-01
0.1400E 02	0.	-0.	0.	0.7569E-03	0.4253E-03	0.9263E-08	0.3719E 03	0.3637E 04	0.7333E-01
0.1600E 02	0.	-0.	0.	0.6507E-03	0.4768E-03	0.8210E-08	0.4183E 03	0.4090E 04	0.7322E-01
0.1800E 02	0.	-0.	0.	0.5516E-03	0.5106E-03	0.7194E-08	0.4624E 03	0.4521E 04	0.7312E-01
0.2000E 02	0.	-0.	0.	0.4617E-03	0.5266E-03	0.6241E-08	0.5042E 03	0.4929E 04	0.7303E-01
0.2200E 02	0.	-0.	0.	0.3823E-03	0.5264E-03	0.5368E-08	0.5436E 03	0.5315E 04	0.7295E-01

DESCENDING

NOZZLE HEIGHT (FT) = 0.3000000E 04 TIME = 2.0000
MOMENTUM FACTOR A = 0.89785561E-01 STAGNATION PRESSURE (PSI) = 0.22346237E-02

DESCENDING

NOZZLE HEIGHT (FT) = 0.2000000E-02 TIME = 4.0000
MOMENTUM FACTOR A = 0.7401685E-01 STAGNATION PRESSURE (PSI) = 0.50279035E-02

STATION (FT)	DEPTH (FT)	SLOPE (DEG)	RATE (FT/SEC)	SURF. PRESS. (PSI)	DYN. PRESS. (PSI)	GAS DENS. SLUG/CU FT	PART. VEL. (FT/SEC)	GAS VEL. (FT/SEC)	TOTAL PRESS. (PSI)
0.1000E-04	C.	0.2848E-03	0.	0.5028E-02	-0.	-0.	-0.	-0.	0.7760E-01
0.2000E 01	0.	-0.9973E-04	0.	0.4808E-02	0.2162E-03	0.5334E-07	0.7997E 02	0.1080E 04	0.7738E-01
0.4000E 01	0.	0.1588E-02	0.	0.4215E-02	0.7570E-03	0.4801E-07	0.1577E 03	0.2131E 04	0.7678E-01
0.6000E 01	0.1445E-04	0.4867E-02	0.4735E-04	0.3412E-02	0.1376E-02	0.4056E-07	0.2314E 03	0.3126E 04	0.7598E-01
0.8000E 01	0.7652E-04	0.5065E-02	0.6751E-04	0.2579E-02	0.1843E-02	0.3243E-07	0.2994E 03	0.4046E 04	0.7515E-01
0.1000E 02	0.4938E-04	0.2454E-C3	0.6733E-04	0.1842E-02	0.2050E-02	0.2479E-07	0.3612E 03	0.4880E 04	0.7441E-01
0.1200E 02	0.5125E-04	-0.5927E-04	0.5657E-04	0.1261E-02	0.2011E-02	0.1831E-07	0.4163E 03	0.5624E 04	0.7383E-01
0.1400E 02	0.4501E-04	-0.2502E-03	0.4193E-04	0.8361E-03	0.1807E-02	0.1319E-07	0.4649E 03	0.6281E 04	0.7341E-01
0.1600E 02	0.3408E-04	-0.2552E-03	0.27741E-04	0.5431E-03	0.1525E-02	0.9344E-08	0.5074E 03	0.6855E 04	0.7311E-01
0.1800E 02	0.2133E-04	-0.3752E-03	0.1436E-04	0.2484E-03	0.1231E-02	0.6556E-08	0.5444E 03	0.7355E 04	0.7292E-01
0.2000E 02	0.8992E-05	-0.2191E-03	0.4863E-05	0.2224E-03	0.9548E-03	0.4580E-08	0.5765E 03	0.7789E 04	0.7279E-01
0.2200E 02	0.9383E-C8	-0.1757E-03	0.	0.1419E-03	0.7406E-03	0.3199E-08	0.6044E 03	0.8165E 04	0.7271E-01

APPENDIX B. JET TURNING ANGLE

In Appendix A, a modification to Roberts' surface loading theory was incorporated through the parameter n to account for the focusing effect of the jet when the gas expands into a nonzero pressure. If such a modification is found to be suitable when the necessary test data becomes available, it is believed that n would depend in some manner on the angle at which the jet is turned when it leaves the nozzle exit lip. During this investigation, the angle through which the jet would be turned while expanding into a perfect vacuum and a Martian environment was examined. The results of this investigation are presented here even though they had little influence on the soil erosion computations performed.

According to References 4 and 5, the jet turning angle δ is given by Figure B1 and (with a change in notation)

$$\delta = v_1 - v_e + \theta_e \quad (B1)$$

where

v_1 = Prandtl-Meyer turning angle corresponding to the ambient stagnation pressure ratio

v_e = Prandtl-Meyer turning angle corresponding to the nozzle exit Mach number

θ_e = nozzle exit half-cone angle

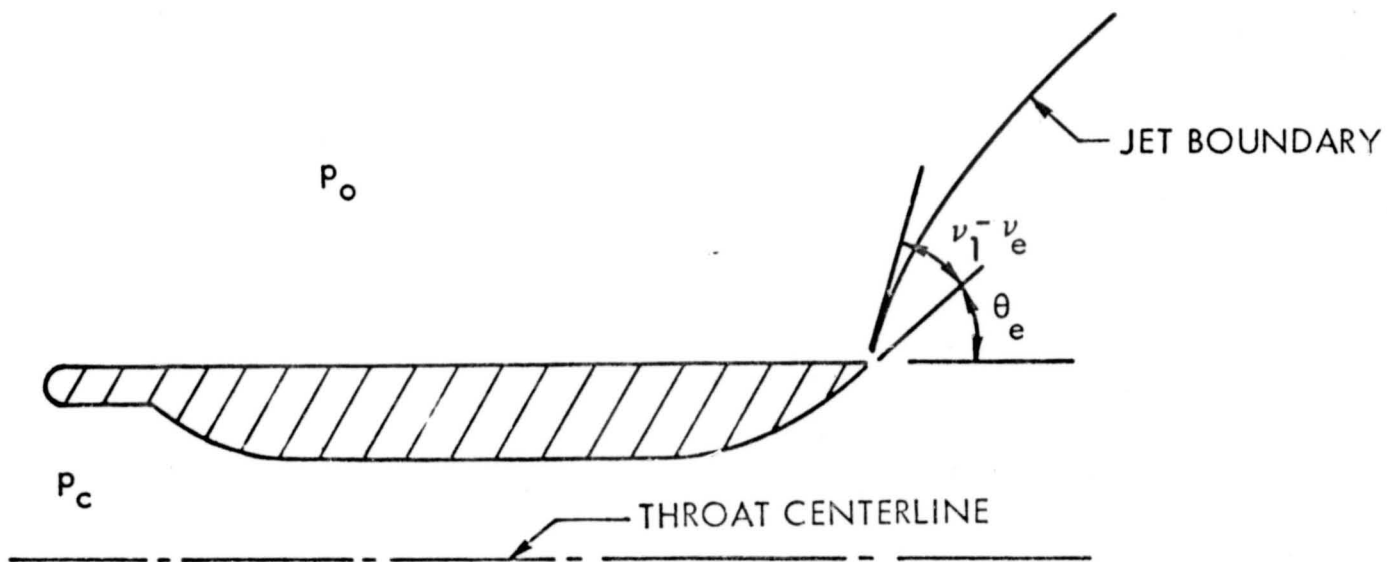


Figure B1. Jet Turning Angle Geometry

The equations given for v_1 and v_e are

$$v_1 = \sqrt{\frac{\gamma+1}{\gamma-1}} \tan^{-1} \sqrt{\frac{\gamma-1}{\gamma+1} (M_1^2 - 1)} - \tan^{-1} \sqrt{M_1^2 - 1} \quad (B2)$$

$$v_e = \sqrt{\frac{\gamma+1}{\gamma-1}} \tan^{-1} \sqrt{\frac{\gamma-1}{\gamma+1} (M_e^2 - 1)} - \tan^{-1} \sqrt{M_e^2 - 1} \quad (B3)$$

where

$$M_1 = \frac{2}{\gamma-1} \left[\left(\frac{p_c}{p_o} \right)^{\frac{\gamma-1}{\gamma}} - 1 \right] \quad (B4)$$

and the additional parameters are defined as

M_e = exit Mach number (dimensionless)

p_c = chamber gas pressure (psf)

p_o = ambient pressure (psf)

γ = gas specific heat ratio (dimensionless)

In a perfect vacuum ($p_o = 0$) the jet turning angle becomes

$$\nu = \frac{\pi}{2} \left[\sqrt{\frac{\gamma+1}{\gamma-1}} - 1 \right] + \theta_e \text{ (radians)} \quad (B5)$$

The solution of Equation (B5) is shown in Figure B2 for a range of gas specific heat ratios, and the solution of Equation (B1) is shown in Figure B3 for a range of ambient pressures for several specific heat ratios. For example, according to Figure B2 for a specific heat ratio of 1.252, the turning angle in a perfect vacuum would be about 114 degrees. Whereas, while expanding into a Martian ambient pressure of 0.0726 psi, the turning angle is approximately 24.6 degrees. These calculations suggest that the surface pressures under the Martian ambient pressures should be higher at the stagnation point and be confined to a smaller region on the surface than if the jet expanded into a perfect vacuum. The specific dependence of n , if one actually exists, upon these turning angles can be investigated when surface pressure test data become available.

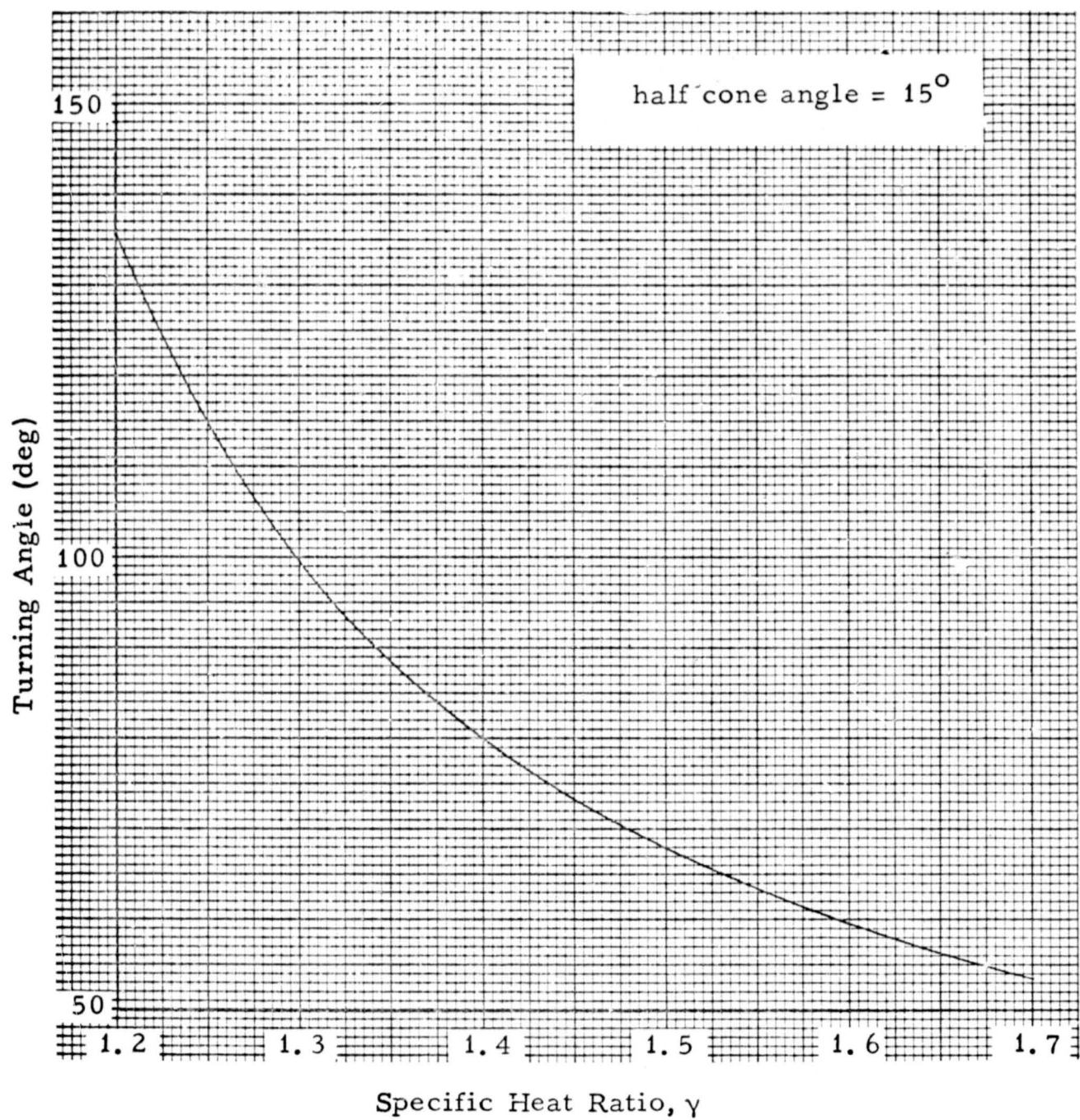


Figure B2. Variation of Turning Angle with Specific Heat Ratio-
Expanding Into a Perfect Vacuum

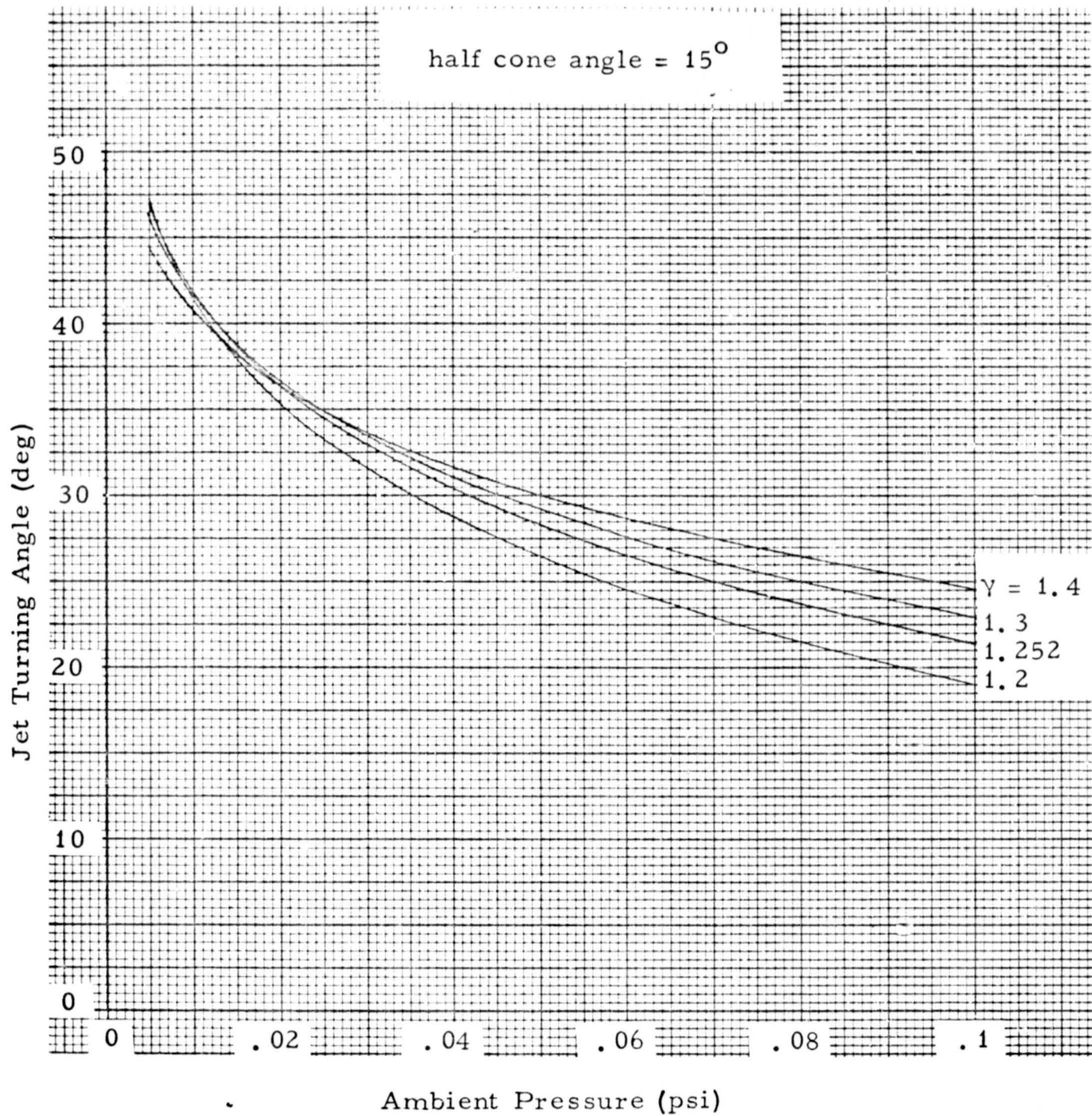


Figure B3. Variation of Jet Turning Angle With Ambient Pressure and Gas Specific Heat Ratio

APPENDIX C. PARTICLE TRAJECTORIES

This appendix considers the motion of a particle ejected from a horizontal plane surface at velocity V and angle β with the surface. After ejection the particle moves under the action of gravitational and aerodynamic drag forces. The objective of the analysis is to determine the particle impact point. The motivation for performing this analysis is because small soil particles can attain a large fraction of the gas velocity. Then, at such large velocities, their subsequent motion can be drastically altered by the presence of an atmosphere.

Figure C1 shows a typical particle trajectory. The symbols and the coordinate system used in the analysis are defined as follows:

A = particle cross-sectional area (ft^2)

C_D = aerodynamic drag coefficient (dimensionless)

D = particle diameter (ft)

K = drag parameter (ft^{-1})

m = particle mass (slugs)

r = particle radial displacement from point of ejection (ft)

R = particle range in an atmosphere (ft)

R_0 = particle range in a vacuum (ft)

t_1 = time to reach maximum height, y_m (sec)

t_2 = duration of flight (sec)

u_o = horizontal component of initial velocity = $V \cos \beta$ (ft/sec)

v_o = vertical component of initial velocity = $V \sin \beta$ (ft/sec)

v_2 = vertical velocity at impact (ft/sec)

V = particle ejection velocity (ft/sec)

y = particle vertical displacement from point of ejection (ft)

y_m = maximum height (ft)

β = angle at which particle leaves surface (rad)

ρ = atmosphere mass density (slugs/ft³)

σ = particle mass density (slugs/ft³)

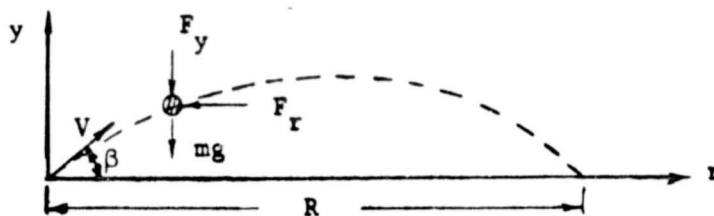


Figure C1: Typical Particle Trajectory Showing Gravity and Aerodynamic Forces

1. Particle Motion in a Vacuum

The equations of motion of a particle in the r direction in a vacuum is

$$\left. \begin{array}{l} m \ddot{r} = 0 \\ r(0) = 0, \dot{r}(0) = u_0 = V \cos \beta \end{array} \right\} \quad (C1)$$

and in the y direction is

$$\left. \begin{array}{l} m \ddot{y} = -mg \\ y(0) = 0, \dot{y}(0) = v_0 = V \sin \beta \end{array} \right\} \quad (C2)$$

The solution of these equations are

$$\left. \begin{array}{l} r = u_0 t \\ y = v_0 t - \frac{1}{2} g t^2 \end{array} \right\} \quad (C3)$$

Eliminating time the trajectory becomes

$$y = r \tan \beta - \frac{gr^2}{2V^2 \cos^2 \beta} \quad (C4)$$

From (C3) and (C4) one finds that

$$y_m = \text{maximum height} = \frac{1}{2} \frac{v_0^2}{g} \quad (C5)$$

$$t_1 = \text{time to reach maximum height} = \frac{v_0}{g} \quad (C6)$$

$$R_o = \text{range} = \frac{v_0^2 \sin 2\theta}{g} \quad (C7)$$

$$t_2 = \text{total flight time} = \frac{2v_0}{g} \quad (C8)$$

$$v_2 = \text{vertical velocity at impact} = -v_0 \quad (C9)$$

2. Particle Motion in an Atmosphere

To account for the atmospheric drag forces one must assume a particle shape and the drag force law. It is assumed the drag force is proportional to the square of the velocity component and that the particles are spherical.

(a) Motion in r Direction

The equation of motion for the r direction is

$$\ddot{r}_r = -\frac{1}{2} \rho A C_D \dot{r}^2 \quad (C10)$$

subject to the same initial conditions as the drag free case.

Now with

$$m = \frac{\pi D^3 \sigma}{6}, \quad A = \frac{\pi D^2}{4} \quad (C11)$$

one has

$$\ddot{r}_r = -K \dot{r}^2 \quad (C12)$$

where

$$K = \frac{3}{4} \frac{\rho C_D}{\sigma D} \quad (C13)$$

The solution of (C12) satisfying the initial conditions is

$$r = \frac{1}{K} \ln (1 + Ku_0 t) \quad (C14)$$

(b) Motion in y Direction

For motion in the y direction it is convenient to separate the total flight time into two periods; one in which the particle is ascending and the second when it is descending. During the upward motion the drag force, which opposes the velocity, acts downward, and therefore is a negative force acting on the particle. During the downward motion the drag force, which again opposes the velocity, acts upward, and therefore is a positive force acting on the particle. The initial conditions are:

$$t = 0, y = 0, \dot{y} = + v_0 \quad (C15)$$

and at the end of the ascent phase (at time $t = t_1$) the conditions are:

$$t = t_1, y = y_m, \dot{y} = 0 \quad (C16)$$

At the end of the descent phase (at time $t = t_2$) when the particle impacts the plane the conditions are:

$$t = t_2, y = 0, \dot{y} = v_2 \quad (C17)$$

Ascent Phase

The equation of motion is

$$m\ddot{y} = - \frac{1}{2} \rho A C_D \dot{y}^2 - mg$$

or

$$\ddot{y} = - \frac{1}{2} K \dot{y}^2 - g \quad (C18)$$

Replacing \ddot{y} by

$$y = \dot{y} \frac{dy}{d\dot{y}} = \frac{1}{2} \frac{dy^2}{d\dot{y}} \quad (C19)$$

and solving for y as a function of the velocity \dot{y} for the initial conditions given in (C15) gives

$$y = \frac{1}{2K} \ln \left(\frac{\frac{Kv_o^2}{g}}{1 + \frac{Kv}{g}} \right)^2 \quad (C20)$$

From (C20) the maximum upward displacement is found to be (occurs when $\dot{y} = 0$)

$$y_m = \frac{1}{2K} \ln \left(1 + K \frac{v_o^2}{g} \right)^2 \quad (C21)$$

The velocity \dot{y} for any displacement y is

$$\dot{y} = v_o \sqrt{ \left(1 + \frac{g}{Kv_o^2} \right) e^{-2Ky} - \frac{g}{Kv_o^2} } \quad (C22)$$

Upon separation of variables (C22) can be placed in the form

$$\sqrt{\frac{dy}{A^2 e^{-2Ky} - 1}} = \sqrt{\frac{g}{K}} dt \quad (C23)$$

where

$$A = \sqrt{1 + \frac{Kv_o^2}{g}} \quad (C24)$$

Integration of (C23) gives

$$\frac{1}{2} t \sqrt{gk} = \tan^{-1} \left\{ \frac{A + \sqrt{A^2 - 1} - Ae^{-Ky} - \sqrt{A^2 e^{-2Ky} - 1}}{1 + (A + \sqrt{A^2 - 1})(Ae^{-Ky} + \sqrt{A^2 e^{-2Ky} - 1})} \right\} \quad (C25)$$

The time $t = t_1$, when the particle reaches the maximum height corresponds to $y = y_m$. Using the definition of A given by (C24) equation (C21) becomes

$$y_m = \frac{1}{2K} \ln (A^2) = \frac{1}{K} \ln (A) \quad (C26)$$

or

$$Ky_m = \ln (A)$$

and

$$e^{-Ky_m} = \frac{1}{A}, \quad e^{-2Ky_m} = \frac{1}{A^2}$$

Using these results the time t_1 determined from (C25) becomes

$$\frac{1}{2} t_1 \sqrt{gK} = \tan^{-1} \left(\frac{A-1 + \sqrt{A^2-1}}{A+1 + \sqrt{A^2-1}} \right)$$

After a few algebraic manipulations the argument of the inverse tangent function can be written as

$$\frac{A-1 + \sqrt{A^2-1}}{A+1 + \sqrt{A^2-1}} = \frac{A-1}{B}$$

where

$$B = v_o \sqrt{\frac{K}{g}} \quad (C27)$$

and therefore the time t_1 becomes

$$t_1 = \frac{2}{\sqrt{gK}} \tan^{-1} \left(\frac{A-1}{B} \right) \quad (C28)$$

Descent Phase

The equation of motion for the descent phase is

$$\ddot{my} = + \frac{1}{2} \rho A C_D \dot{y}^2 - mg$$

or

$$\ddot{y} = Ky^2 - g \quad (C29)$$

Proceeding along steps similar to those during the ascent phase, the first integral of (C29) is

$$-\frac{g}{K} \ln \left(1 - \frac{Ky^2}{g} \right) = -2gy + C_1$$

where C_1 is a constant of integration. This constant is determined such that

$$y = y_m, y = 0, t = t_1$$

and the solution becomes

$$y = \frac{1}{2K} \ln \left[A^2 \left(1 - \frac{Ky^2}{g} \right) \right] \quad (C30)$$

The impact velocity can be determined from (C30) by setting

$y = 0$ and $y = v_2$. The result is

$$v_2 = -\sqrt{\frac{g}{K} \frac{A^2 - 1}{A^2}}$$

from which one finds that

$$v_2 = -\frac{v_0}{A} \quad (C31)$$

Returning to (C30) and solving for y gives

$$y = \pm \sqrt{\frac{g}{K}} \frac{\sqrt{A^2 e^{-2Ky} - 1}}{A e^{-Ky}} \quad (C32)$$

Since y is negative during the downward motion, one takes the negative sign. Separating variables yields

$$\frac{Ae^{-Ky} dy}{\sqrt{A^2 e^{-2Ky} - 1}} = -\sqrt{\frac{g}{K}} dt \quad (C33)$$

and then integration of (C33) gives

$$-\frac{1}{AK} \cosh^{-1} (Ae^{-Ky}) = -\frac{1}{A\sqrt{K}} t + C_2$$

where C_2 is a constant of integration. This constant is determined such that at

$$t = t_1, y = y_m$$

and the solution becomes

$$t = \frac{1}{\sqrt{gK}} \left\{ \cosh^{-1} (Ae^{-Ky}) + 2 \tan^{-1} \left(\frac{A-1}{B} \right) \right\} \quad (C34)$$

The time $t = t_2$ at which the particle impacts the ground is obtained from (C34) by setting $y = 0$. Making use of the relation

$$\cosh^{-1}(A) = \ln \left(A + \sqrt{A^2 - 1} \right) = \ln(A+B) \text{ the time } t_2 \text{ becomes}$$

$$t_2 = \frac{1}{\sqrt{gK}} \left\{ \ln(A+B) + 2 \tan^{-1} \left(\frac{A-1}{B} \right) \right\} \quad (C35)$$

The corresponding range is now obtained by substituting this value of $t = t_2$ into (C14) to obtain

$$R = \frac{1}{K} \ln (1 + Ku_0 t_2) \quad (C36)$$

One can readily verify that these solutions reduce to those obtained for t_1 , y_m , t_2 , v_2 and R for the drag free case, if the

series expansion (valid for small K)

$$t_2 = \frac{2v_o}{g} - \frac{7}{12} \frac{v_o^3}{g^2} K + O(K^2)$$

is introduced and the limit taken as K approaches zero.

(c) Summary

The corresponding equations listed in (C5) through (C9) obtained for the drag free case become the following for the case when aerodynamic drag is considered:

$$\left. \begin{aligned} v_m &= \frac{1}{2K} \ln(1 + Kv_o^2/g) \\ t_1 &= \frac{2}{\sqrt{gK}} \tan^{-1} \left(\frac{A-1}{B} \right) \\ R &= \frac{1}{K} \ln(1 + Ku_o t_2) \\ t_2 &= \frac{1}{\sqrt{gK}} \left\{ 2 \tan^{-1} \left(\frac{A-1}{B} \right) + \ln(A+B) \right\} \\ v_2 &= \pm \sqrt{\frac{g}{K} \left(\frac{A^2-1}{A^2} \right)} \end{aligned} \right\} \quad (C37)$$

where

$$\left. \begin{aligned} A &= \sqrt{1 + \frac{Kv_o^2}{g}}, \quad B = v_o \sqrt{\frac{K}{g}} \\ K &= \frac{3}{4} \frac{\rho C_D}{\sigma D} \end{aligned} \right\} \quad (C38)$$

An indication of the effect of the aerodynamic drag on the range is provided by the nondimensional plot shown in Figure C2.

This figure shows the ratio of the range in atmosphere to that in a vacuum as functions of the nondimensional parameters.

$$a = \frac{Kv_o^2}{g} = \frac{3}{4} \frac{\rho C_D v^2}{\sigma D g} \cos^2 \beta$$

$$b = \frac{Ku_o^2}{g} = \frac{3}{4} \frac{\rho C_D v^2}{\sigma D g} \sin^2 \beta$$

(d) Estimate of Drag Coefficient

In an effort to estimate the drag coefficient calculations of range were made and compared with experimental data listed in Reference 6. On page 401 of Reference 6 the following data for a .30 caliber bullet are listed.

nozzle velocity = 2700 ft/sec

diameter = .308 inches

range = 500 yards, angle = 15.6 minutes (.260 deg)

range = 1000 yards, angle = 49.4 minutes (.823 deg)

Taking the air density to be 0.002378 slugs/ft³ and the density of the projectile to be 22.06 slugs/ft³ the equations derived in this appendix yielded the following results.

Angle β (deg)	Actual Range (ft)	Theoretical Range (ft)		
		$C_D = 0$	$C_D = .14$	$C_D = .15$
0.260	1500	2055	1462	1435
0.823	3000	6506	3060	2965

From these calculations a representative value of the drag coefficients was assumed to be $C_D = .14$.

C-11

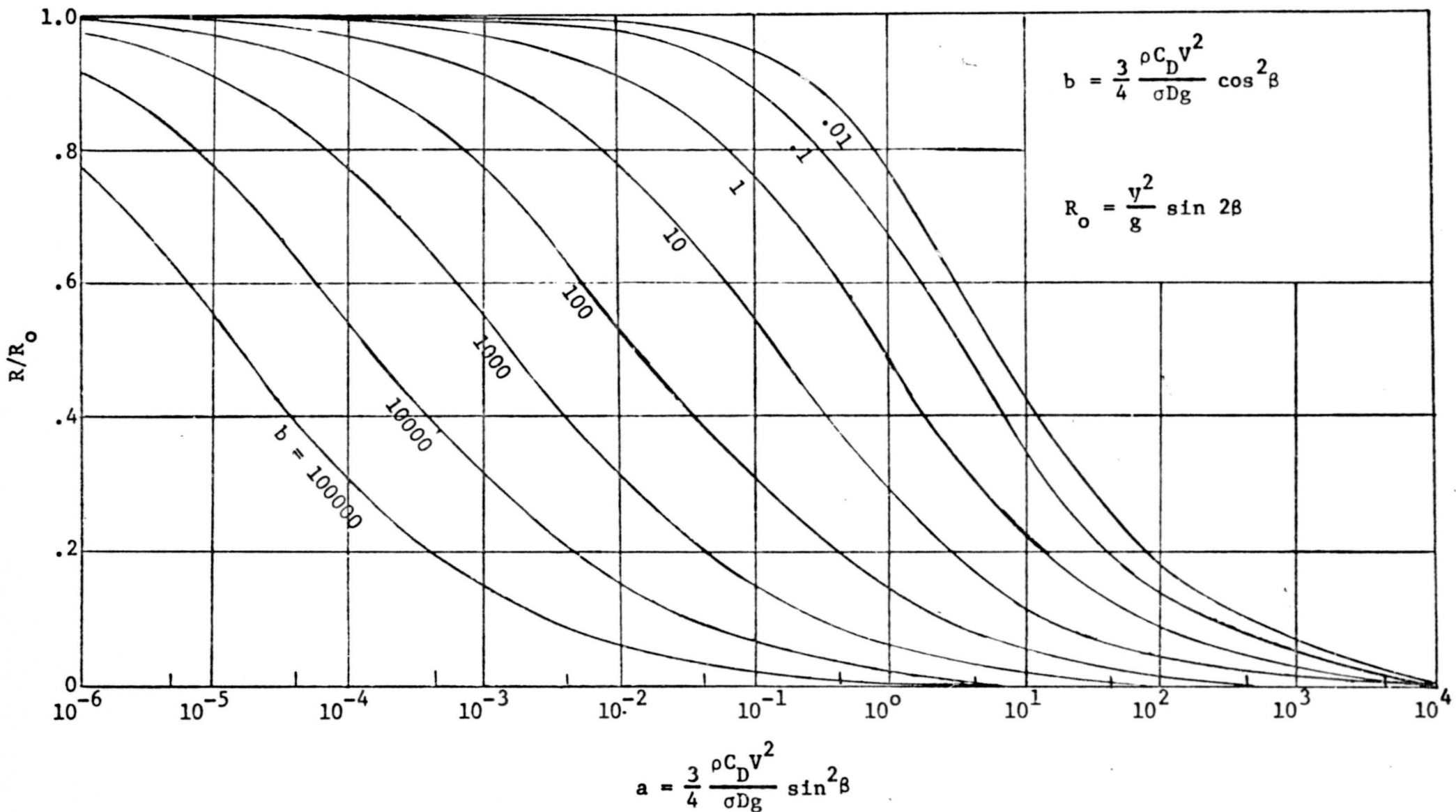


Figure C2. Particle Range Including Aerodynamic Drag